



## Late to post-Variscan differential uplift and basement segmentation along the SW Bohemian Massif, Central Europe

Andreas Eberts<sup>1</sup>, Hamed Fazlikhani<sup>1</sup>, Wolfgang Bauer<sup>1</sup>, Harald Stollhofen<sup>1</sup>, Helga de Wall<sup>1</sup>, Gerald Gabriel<sup>2,3</sup>

5 <sup>1</sup>GeoZentrum Nordbayern, Friedrich-Alexander-Universität (FAU) Erlangen-Nürnberg, Schlossgarten 5, 91054 Erlangen, Germany.

<sup>2</sup>Leibniz-Institut für Angewandte Geophysik, Stilleweg 2, 30655 Hannover, Germany.

<sup>3</sup>Institut für Geologie, Leibniz Universität Hannover, Callinstraße 30, 30167 Hannover, Germany.

*Correspondence to:* Andreas Eberts (andreas.eberts@outlook.de)

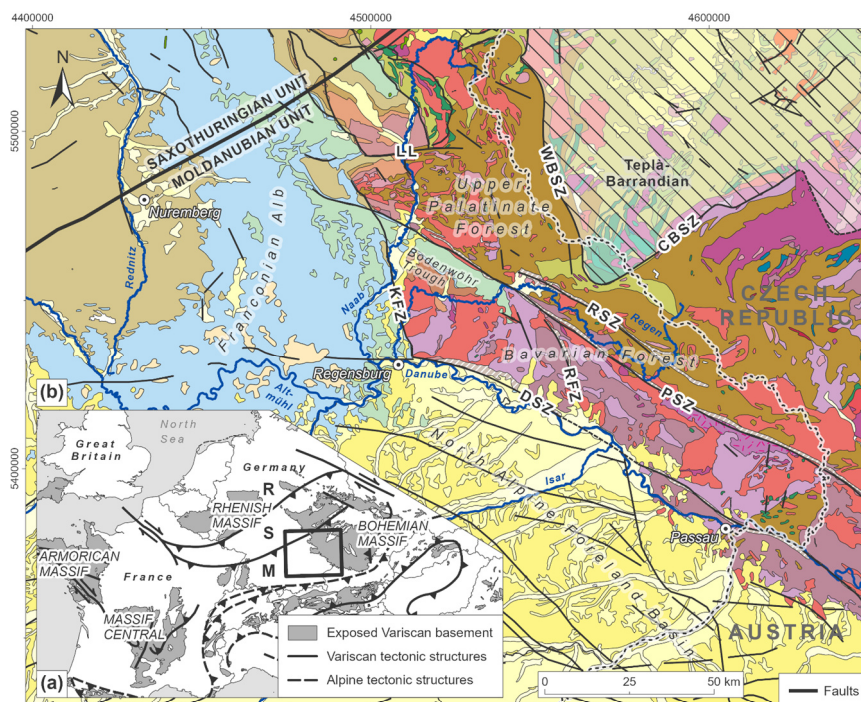
10 **Abstract.** The exposed Variscan basement in Central Europe is well-known for its complex structural and lithological architecture resulting from multiple deformation phases. We study the southwestern margin of the Bohemian Massif, which is characterized by major and long-lived shear zones, such as the Pfahl and Danube shear zones, extending over >100 km and initiated during Variscan tectonics. We integrate Bouguer gravity anomaly and LiDAR topographic data analyses and combine our results with available data and observations from low-temperature thermochronology, metamorphic grades, and granite intrusion depths to detect patterns of basement block segmentation and differential uplift. Three NW-SE striking basement blocks are bordered by the Runding, Pfahl, and Danube shear zones from the northeast to the southwest. Basement block boundaries are indicated by abrupt changes in measured gravity patterns and metamorphic grades. By applying high-pass filters to gravity data in combination with lineament analysis, we identified a new NNW-SSE striking tectonic structure (Cham Fault), which further segments known basement blocks. Basement blocks that are segmented by the Cham Fault differ in the abundance and spatial distribution of exposed late Variscan granites and are further characterized by variations of apparent thermochronological age data. Based on our observations and analyses, a differential uplift and tectonic tilt model is proposed to explain the juxtaposition of different crustal levels exposed at the surface. Block segmentation along the NW-SE striking Pfahl and Runding shear zones most likely occurred prior, during, and after late-orogenic granite emplacement at ca. 320±10 Ma, as some of the granites are cross-cut by the shear zones while others utilized these structures during magma ascent and emplacement. In contrast, activity and block segmentation along the Cham Fault occurred after granite emplacement as the fault sharply truncates the granite inventory. Our study provides evidence for intense and continuous fault activity during late and early post-orogenic times and highlights the importance of tectonic structures in the juxtaposition of different crustal levels and the creation of complex lithological patterns in orogenic terrains.

15  
20  
25



## 1 Introduction

30 The Bohemian Massif extends over ca. 90,000 km<sup>2</sup> and represents one of the largest coherent exposures of Variscan basement rocks in Western and Central Europe. Originating from the collision of the Laurussia and Gondwana supercontinents during the Paleozoic, the Variscan Orogen formed a belt of low- to high-grade metamorphic and plutonic rocks (summary in Schulmann et al., 2014; Fig. 1a).



### Main geological units

#### Sedimentary cover

Quaternary	Fluvial sands and gravels
	Glacial silts, sands, and gravels
Tertiary	Residual fluvial and lacustrine deposits
	Fluvial and lacustrine clays, sands, and gravels
Cretaceous	Carbonates, marl-, clay-, and sandstones
Jurassic	Marine carbonates, marl-, clay-, and sandstones
Triassic	Marine to terrestrial clay- and sandstones
	Marine carbonates, clay-, marl-, and dolostones
Permian	Fluvial clay-, silt-, and sandstones
	Fluvial clay- and sandstones

#### Moldanubian basement

Upper Carboniferous to Triassic	Fault rocks
Carboniferous	Granites
	Dykes
Lower Carboniferous	Diorites and granodiorites
	Dark diatexites (Palit-Komplex)
Neoproterozoic to lower Carboniferous	Diatexite
	Diatexites and gneisses
Neoproterozoic to upper Paleozoic	Schists and phyllites
	Paragneisses
	Orthogneisses

35 **Figure 1 (a)** Main areas exposing Variscan basement rocks in Central Europe, including traces of major Variscan and Alpine tectonic structures (compiled from Matte, 1986; Franke, 1989; Neubauer and Handler, 2000; Barrier et al., 2004; Asch, 2005). **(b)** Geological and tectonic framework of the southwestern Bohemian Massif (compiled from Freudenberger and Schwerd, 1996; Toloczyki et al., 2006; Teipel et al., 2008; Galadí-Enríquez et al., 2009b). Variscan zones: *R* Rhenohercynian Zone, *S* Saxothuringian Zone, *M* Moldanubian Zone. Fault zones: *CBSZ* Central Bohemia Shear Zone, *DSZ* Danube Shear Zone, *KFZ* Keilberg Fault Zone, *LL* Luhe Line, *PSZ* Pfahl Shear Zone, *RSZ* Runding Shear Zone, *RFZ* Rattenberg Fault Zone, *WBSZ* West Bohemia Shear Zone.

40



Variscan convergence was followed by widespread strike-slip faulting during the late-orogenic evolution between ca. 360 and 320 Ma (e.g., Echtler and Chauvet, 1992; Krohe, 1996; Stephan et al., 2016). As a result, the Bohemian Massif hosts some of the most important fault zones of Central Europe, such as the NW-SE striking Pfahl and Danube shear zones (Fig. 1b). Multiple phases of tectonic activity during the Permian to Paleogene initiated new sets of brittle faults and reactivated pre-existing ductile and brittle structures, creating complex structural patterns (e.g., Horn et al., 1986; Meyer, 1989; Wallbrecher et al., 1991; Kley and Voigt, 2008; Siebel et al., 2010; Schaarschmidt et al., 2019).

The outlined relatively simple succession of tectonic events does not reflect the real complexity of the Bohemian Massif's structure, juxtaposing high-grade metamorphic domains (e.g., the Moldanubian Unit) against low-grade domains (e.g., the Teplá-Barrandian Unit, Krohe, 1996; Cymerman et al., 1997; Kroner et al., 2008). At the local scale, complex lithological and metamorphic patterns can also be observed within each metamorphic unit (Krohe, 1996), which is especially evident in the Moldanubian Unit along the southwestern Bohemian Massif (Fig. 1b). Several studies have contributed to the deciphering of the geochronological and geochemical character of that area, especially focusing on the magmatic evolution of the granitic intrusions during the late Variscan tectonothermal event (Finger and Clemens, 1995; Chen et al., 2003; Chen and Siebel, 2004; Dietl et al., 2005; Siebel et al., 2006b; Siebel et al., 2008; Klein et al., 2008; Galadí-Enríquez et al., 2010; Finger et al., 2010). However, the causes for the observed juxtaposition of various metamorphic units and the role of fault reactivation and associated upper crustal vertical movements have not yet been investigated in detail.

In this paper, we apply an integrated methodological approach, combining the analysis of filtered gravity data, high-resolution Digital Elevation Models (DEMs), and published thermochronological data to reveal the spatial distribution of exposed Variscan units and their boundaries along the southwestern Bohemian Massif. In this context, we also discuss the role of upper crustal fault zones in the exposure of different crustal levels responsible for the observed juxtaposition of varying lithological domains, the latter being one of the most characteristic features of the entire Variscan Orogen (e.g., Krohe, 1996).

## 2 Geological and tectonic setting of the southwestern Bohemian Massif

The late stages of the Variscan Orogeny were characterized by widespread strike-slip faulting and HT/LP metamorphism (Echtler and Chauvet, 1992; Krohe, 1996; Franke, 2000; Büttner, 2007; Kroner and Romer, 2013; Schulmann et al., 2014; Stephan et al., 2016). Along the southwestern Bohemian Massif, this late-stage evolution of the Variscan Orogeny is manifested by the initiation of crustal-scale fault zones, such as the Pfahl and Danube shear zones, and large-scale crustal melting as seen in vast migmatite complexes intruded by voluminous late- to post-orogenic granite bodies (Wallbrecher et al., 1991; Brandmayr et al., 1995; Finger and Clemens, 1995; Kalt et al., 1999; Kalt et al., 2000; Propach et al., 2000; Chen et al., 2003; Siebel et al., 2003; Klein et al., 2008). Two distinct tectonometamorphic units bounded by large fault zones are (1) the Moldanubian (*sensu stricto*, further referred to as the Moldanubian Unit) and (2) the Teplá-Barrandian (Kossmat, 1927; Franke, 1989; Fig. 1b). The Moldanubian Unit is comprised of high-grade metamorphic rocks predominantly formed during the Var-



75

iscan HT/LP tectonothermal events (e.g., Grauert et al., 1974; Franke, 1989). The Teplá-Barrandian Unit is considered a supracrustal unit consisting of a low-grade Neoproterozoic basement (e.g., Franke, 1989; Žák et al., 2014). In this study, we focus on basement segmentation and crustal uplift of the Moldanubian Unit exposed at the southwestern margin of the Bohemian Massif.

## 2.1 Origin and characteristics of the Moldanubian basement units

During the ceasing Cadomian Orogeny in the late Neoproterozoic/early Paleozoic, the area of the nowadays southwestern Bohemian Massif was situated along the northern margin of Gondwana (e.g., Rohrmüller et al., 1996; Linnemann et al., 2004; Fatka and Mergl, 2009; Žák and Sláma, 2018). A succession of mainly pelitic greywackes, intercalated with magmatites, are thereby considered as the protoliths of the so-called “Monotonous Group”. The latter is characterized by a series of biotite-plagioclase-bearing para- and orthogneisses with an only minor abundance of quartzites, marbles, graphitic schists, amphibolites, and granitic gneisses (Rohrmüller et al., 1996; Franke, 2000; Kroner et al., 2008). On the other hand, volcano-sedimentary successions, probably formed in response to continental rifting and associated volcanism, are documented within the so-called “Varied Group”. This group is characterized by paragneisses with higher abundances of quartzites, marbles, graphitic schists, and amphibolites (Rohrmüller et al., 1996; Kroner et al., 2008).

Late Neoproterozoic/early Paleozoic units of the southwestern Bohemian Massif were overprinted by HT/LP metamorphism during the late stages of the Variscan Orogeny. Pressures of up to 7 kbar (i.e., ca. 20 km burial depth) and temperatures of >800 °C led to partial melting and the formation of vast migmatite complexes (Grauert et al., 1974; Kalt et al., 1999; Kalt et al., 2000), the anatexis grade of which is increasing from the northeast to the southwest (Blümel, 1972; Teipel et al., 2008; Galadí-Enríquez et al., 2009b). Whereas this metamorphic event has been dated to ca. 335 to 340 Ma in the southern central Bohemian Massif, younger thermal overprint and partial anatexis are documented for the Bavarian part of the Moldanubian Unit, with metamorphic ages progressively decreasing towards the southwest (ca. 320 to 315 Ma in the area to the southwest of the Pfahl Shear Zone, Kalt et al., 2000; Propach et al., 2000; Gerdes et al., 2006; Finger et al., 2007; Siebel et al., 2012; compiled by Teipel et al., 2008). Contemporaneously, voluminous granite bodies intruded large parts of the southwestern Bohemian Massif (Table 1). Estimates of granite emplacement depths in the study area are restricted to the southeastern Bavarian Forest (Fig. 1b and Table 1). They vary between 14–15 km for the Saldenburg Granite, which is part of the Fürstenstein Composite Massif (Dietl et al., 2005), and 16–18 km for the Hauzenberg Granite II, which is part of the Hauzenberg Composite Massif (Klein et al., 2008). Erosional products of these late-orogenic granites were deposited in the adjacent Permian basin (Naab Trough *sensu* Schröder, 1988), indicating their rapid exhumation and erosion shortly after their Upper Carboniferous to early Permian emplacement (Mielke, 1993; Galadí-Enríquez et al., 2009a).



105

**Table 1** Ages and emplacement depths for granites along the southwestern Bohemian Massif. All ages have been measured on zircons. For granite locations, see Fig. 3. <sup>a</sup>Klein et al. (2008), <sup>b</sup>Chen and Siebel (2004), <sup>c</sup>Dietl et al. (2005), <sup>d</sup>Siebel et al. (2008), <sup>e</sup>Siebel et al. (2006a), <sup>f</sup>Siebel et al. (2010), <sup>g</sup>Chen et al. (2003). *ND* not determined.

Name	Variety	Age (Ma), method	Min. emplacement depth (km)
Hauzenberg Composite Massif	<i>Hauzenberg Granite II</i>	320±3 <sup>a</sup> , U-Pb	16-18 <sup>a</sup>
Fürstenstein Composite Massif	<i>Tittling Granite</i>	322-324 <sup>b</sup> , Pb-Pb	ND
	<i>Eberhardsreuth Granite</i>	312-316 <sup>b</sup> , Pb-Pb	ND
	<i>Saldenburg Granite</i>	312-318 <sup>b</sup> , Pb-Pb	14-15 <sup>c</sup>
Haidel Massif		323±4 <sup>d</sup> , Pb-Pb	ND
Rinchnach Stock		320-329 <sup>e</sup> , Pb-Pb	ND
Patersdorf Stock		322-323 <sup>e</sup> , Pb-Pb	ND
Metten Massif		324±5 <sup>d</sup> , Pb-Pb	ND
Arnbruck Stock		325±2 <sup>d</sup> , Pb-Pb	ND
Regensburg Forest Massif	<i>Kristallgranit</i>	325±7 <sup>f</sup> , Pb-Pb	ND
Neunburg Massif		319±4 <sup>g</sup> , U-Pb	ND
Oberviechtach Stock		ca. 320 <sup>g</sup> , U-Pb	ND

## 2.2 Structural characteristics

The tectonic configuration of the southwestern Bohemian Massif during the late stages of the Variscan Orogeny is interpreted as a conjugate shear system related to N to NNW directed shortening (Wallbrecher et al., 1991; Brandmayr et al., 1995; Galadí-Enríquez et al., 2010). The NW-SE trending Pfahl Shear Zone strikes over 150 km from northern Austria to southeast Germany; it is the best-known and one of the most prominent examples among the resulting dextral strike-slip faults (e.g., Brandmayr et al., 1995; Table 2). The Pfahl Shear Zone marks a pronounced change in the anatectic grade, separating the metatectic-dominated domain of the northeastern Bavarian and Upper Palatinate forests from the diatectic-dominated domain of the southwestern Bavarian Forest (Teipel et al., 2008; Galadí-Enríquez et al., 2009b; Fig. 1b). Changes in anatectic grades and variations of the granite geochemistry across the Pfahl Shear Zone are interpreted as reflecting differential uplift with deeper crustal levels exposed to the southwest of the shear zone (Grauert et al., 1974; Beer, 1981; Finger and Clemens, 1995; Siebel et al., 2008; Finger and Rene, 2009). In addition, analysis of quartz mineralizations along the Pfahl Shear Zone gives an indication for the exposure of deeper crustal levels along the southeastern segment of the shear zone (Schaarschmidt et al., 2019). Two contrasting interpretations of the origin of the Pfahl Shear Zone exist, i.e., (I) the shear zone represents a former suture zone along which two different basement terranes amalgamated (Siebel et al., 2008; Siebel et al., 2009) or (II) the shear zone just intersects the otherwise continuous Moldanubian Unit (Finger et al., 2007; Finger and Rene, 2009; Finger et al., 2010).



Sub-parallel and ca. 10 km north of the Pfahl Shear Zone, the Runding Shear Zone represents another important tectonic lineament in the study area (Fig. 1b, Table 2). Similar to the Pfahl Shear Zone, the Runding Shear Zone marks a pronounced change in anatectic grades, separating the metatectic-dominated domain of the northeastern Bavarian Forest from higher-grade diatectic rocks in between the Pfahl and Runding shear zones (Teipel et al., 2008; Fig. 1b).

125 In the southwest, the exposed Moldanubian basement is delimited by the Danube Shear Zone (Fig. 1b). Similar to the Pfahl Shear Zone, the Danube Shear Zone is characterized by multiple deformation phases lasting from the late Paleozoic until the Cenozoic (Table 2). The structural grain in between these two major shear zones is interpreted to be related to a dextral Riedel-type shear system that developed in response to a “rift-and-wrench” tectonic phase under a NNW-SSE directed compressional stress field (Zeitlhöfler, 2007).

130 **Table 2** Main inferred tectonic activity phases, kinematics, and minimum displacements of the six major fault zones in the Moldanubian Unit of the southwestern Bohemian Massif. <sup>a</sup>Mattern (1995), <sup>b</sup>Siebel et al. (2010), <sup>c</sup>Freudenberger (1996), <sup>d</sup>Führer (1978), <sup>e</sup>Bauberger and Cramer (1961), <sup>f</sup>Carlé (1955), <sup>g</sup>Seemann (1925), <sup>h</sup>Meyer (1989), <sup>i</sup>Müller (1994), <sup>j</sup>Peterek et al. (1996), <sup>k</sup>Siebel et al. (2005), <sup>l</sup>Galadí-Enríquez et al. (2010), <sup>m</sup>Horn et al. (1986), <sup>n</sup>Meyer (1993), <sup>o</sup>Rohrmüller et al. (2017), <sup>p</sup>Zeitlhöfler (2007). *ND* not determined.

Name	Strike	Inferred activity phase	Main kinematics	Est. displ. (km)
Danube Shear Zone	NW-SE	Carboniferous <sup>a,b</sup> - Permian <sup>b</sup>	Dextral strike-slip <sup>a,b</sup>	ND
		Mesozoic - Cenozoic <sup>b,c</sup>	Normal <sup>d</sup>	1.3 <sup>c</sup>
Keilberg Fault Zone	NNW-SSE	Late Paleozoic - Paleogene <sup>e,f,g</sup>	Reverse <sup>c</sup> , Normal <sup>h</sup>	1.2 <sup>c</sup>
Luhe Line	E-W	Carboniferous - Permian <sup>i</sup>	Reverse <sup>i</sup>	2 <sup>i</sup>
		Lower Cretaceous <sup>j</sup>	Normal <sup>j</sup>	ND
		Upper Cretaceous - Paleogene <sup>j</sup>	Reverse <sup>j</sup>	ND
Pfahl Shear Zone	NW-SE	Carboniferous <sup>k,l</sup>	Dextral strike-slip <sup>a,l</sup>	ND
		Permian <sup>m</sup>	ND	ND
		Upper Cretaceous - Paleogene <sup>n,h</sup>	Reverse <sup>n,h</sup>	0.5 <sup>n</sup>
Rattenberg Fault Zone	NNW-SSE	Late Paleozoic <sup>o</sup>	ND	ND
Runding Shear Zone	NW-SE	Carboniferous - Permian <sup>p</sup>	Dextral strike-slip <sup>o</sup>	ND

### 3 Data and methodology

135 This study uses an integrated approach combining the analysis of Bouguer gravity anomaly data and Digital Elevation Models (DEMs) to unravel the lithological and structural architecture of the exposed Variscan crust in the southwestern Bohemian Massif.



### 3.1 Gravity analysis

The Bouguer gravity dataset is part of a pool of ca. 350,000 reprocessed and merged gravity data points in Germany and surrounding areas with a mean point spacing of 2-3 km and an overall accuracy of  $\pm 100 \mu\text{Gal}$  (Leibniz-Institut für Angewandte Geophysik, 2010; Skiba, 2011). In this study, we compare surface geology with unfiltered and filtered Bouguer gravity anomaly data to identify potential granites in the subsurface and to reveal the spatial relationship to their exposed counterparts. We applied 20 and 30 km wavelength high-pass filters to the Bouguer gravity anomaly data (using Oasis Montaj, ©Seequent) to identify regional and local anomaly sources in the subsurface. The 20 km high-pass filter mainly includes the gravity signature of causative bodies located in the shallower subsurface, while a 30 km high-pass filter also considers somewhat deeper crustal bodies (e.g., Lowrie, 2007). In areas with exposed crystalline rocks, local circular and semi-circular negative gravity anomalies are often related to exposed and buried granites due to the density contrast between granites and the higher-density metamorphic country rocks (e.g., Trzebski et al., 1997; Siebel et al., 1997; Sedlák et al., 2007; Sedlák et al., 2009). To confirm the density difference between granites and surrounding metamorphic rocks, we collected density data from exposed granites and compared these to published metamorphic rock densities. Granite densities were measured by applying a buoyancy technique in isopropanol (Archimedes' principle). Samples were either collected as loose rocks or, if applicable, as drilled cores of two to five centimeters in diameter to ensure “fresh” samples without major cracks.

### 3.2 Topographic analysis

The DEM used in this study is based on LiDAR (Light Detection and Ranging) point clouds acquired by the Bavarian Agency for Digitisation, High-Speed Internet and Surveying. Only the last returned laser pulses have been considered in the dataset so that the final DEM represents the landscape's elevation without being affected by the vegetational cover. Each data point has been georeferenced, referred to the Gauss-Krüger Coordinate System (zone 4) and the German Combined Quasigeoid 2011 (GCG2011) for precise horizontal and vertical positioning, achieving horizontal accuracies of  $\pm 0.5$  m and vertical accuracies of  $\pm 0.2$  m. DEM data were resampled in ArcGIS Pro (©Esri) to a spatial resolution of 10 m, which ensures efficient data processing with sufficient detail to perform lineament mapping and analysis in the study area.

#### 3.2.1 Topographic swath profiles

Traditional elevation profiles along single lines can only image a small fraction of all topographic characteristics, which is related to their small footprint. In contrast, topographic swath profiles are able to illustrate even complex landscapes without neglecting the spatial distribution of important but spatially limited morphological features such as local peaks and troughs (e.g., Telbisz et al., 2013). We used topographic swath profiles to illustrate the overall topographic expression of the study area. Swath profiles are constructed by projecting the elevation data within a rectangular swath onto its longitudinal axis. Depending on the spatial extent of the studied area, the swath can have widths ranging from 100s of meters to 10s of kilometers.



Swath profile data were obtained using the ArcGIS Add-in “SwathProfiler” (Pérez-Peña et al., 2017). We used a fixed swath width of 10 km for all of the profiles. This value is large enough to summarize the present topographic variations adequately while small enough to avoid mixing of morphologies from very different landscapes. Elevation data were sampled along 50 parallel profiles with a step size of 15 m (i.e., 1.5 times the DEM resolution). Important statistical parameters such as the maximum, minimum, and mean elevation can be illustrated simultaneously, providing information about both the general spatial distribution of elevations within an area but also of discrete topographic features such as local peaks and troughs, paleo-surfaces, and incised valleys.

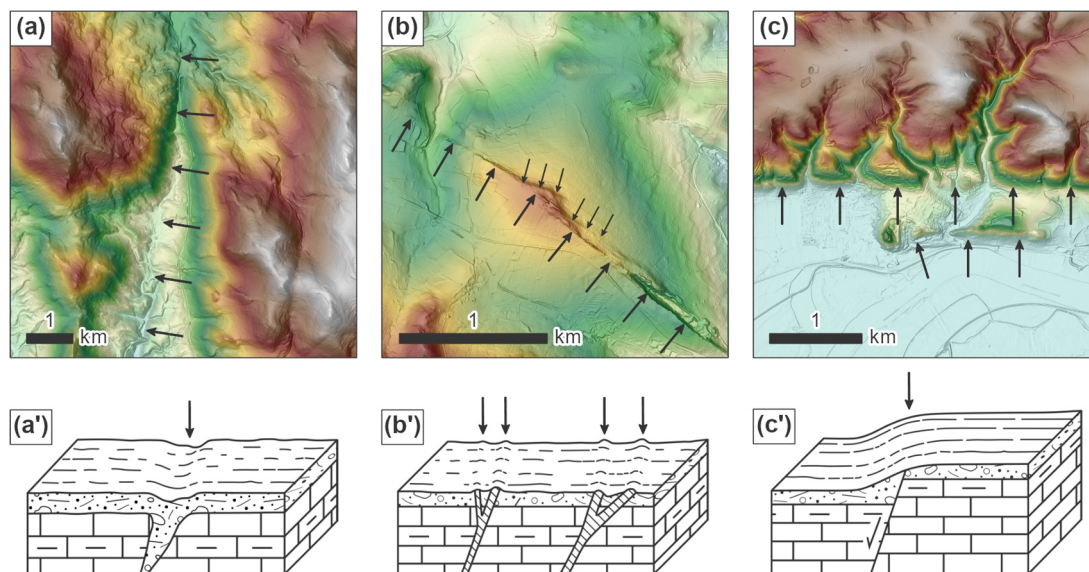
### 3.2.2 Lineament analysis

The analysis of topographic lineaments yields valuable information on the structural patterns of large areas, especially if remote or inaccessible. In cases where active tectonic processes prevail over erosional processes and leveling of the landscape by sediment mobilization and deposition, fault slip is often immediately transferred to the Earth’s surface, forming distinct topographic lineaments (i.e., fault scarps) that can be easily traced and interpreted using aerial photographs, DEMs or field mapping (e.g., Stewart and Hancock, 1990; Keller and Pinter, 2002; Burbank and Anderson, 2012). If the time between fault rupture is long or tectonic activity ceases, however, the scarp will degrade and geomorphic processes will modify the hillslopes and channels of the landscape towards a new equilibrium. In such a case, tectonic structures will no longer be visible as well-defined fault scarps but, because they often induce gradients in rock erodibility, as linear to curvilinear river valleys, ridgelines, or slope breaks (e.g., Jordan et al., 2005; Fig. 2). Strike-slip faults thereby tend to form symmetrical morphologies such as river valleys or ridgelines. High-angle normal and reverse faults typically form linear slope breaks, whereas low-angle thrust faults tend to appear somewhat irregular in topography (Prost, 1994; Drury, 1987; Goldsworthy and Jackson, 2000).

Lineaments were mapped using DEM-derivatives such as hillshade, slope, curvature, and aspect maps as enhancement tools to identify linear features in topography. A shortcoming of traditional hillshade maps is that they induce directional biases due to their heterogeneous way of illuminating the landscape, which is mainly a result of the fixed azimuth of the artificial light source (e.g., Scheiber et al., 2015). To reduce this bias, we used multi-directional hillshades to map topographic lineaments, illuminating landscapes in a more homogenous way.

Calculation of DEM derivatives and the mapping procedure were carried out in ArcGIS Pro (©Esri). Statistical analysis was accomplished by using a modified routine in MATLAB (©Mathworks) that partly relies on the FracPaQ toolbox (Healy et al., 2017).





200  
205

**Figure 2** Map views ((a) to (c)) and sketches ((a') to (c')), after Fürst et al., 1978) illustrating the main lineament geometries encountered along the southwestern Bohemian Massif. Arrows depict the traces of lineaments. (a)-(a') River valleys tend to form along zones of weakened bedrock commonly induced by faults and fractures. The shown example depicts the valley of the river Kollbach located in the Bavarian Forest. (b)-(b') Linear ridgelines may form in cases where minerals, which are more resistant to erosion compared to the adjacent country rocks, have been precipitated within an open fault or fracture system. The most well-known example for this lineament geometry in the study area is the quartz lode of the Pfahl Shear Zone. (c)-(c') Vertical movements along normal and reverse faults are usually expressed as abrupt, linear slope breaks. The shown example is located along the northwestern segment of the Danube Shear Zone.

#### 4 Basement lithological configuration of the southwestern Bohemian Massif

Three main basement domains in the study area are defined based on their dominant metamorphic grades (Fig. 3). Basement domains A, B, and C are bounded by the essentially NW-SE striking Pfahl, Danube, and Runding shear zones (Fig. 3b). By considering the spatial distribution of exposed late Variscan granites, defined basement domains are further subdivided into (1) domains A1, B, and C1, where late Variscan granites are less exposed and are preferentially aligned with NW-SE striking shear zones, and (2) domains A2 and C2, where late Variscan granites are abundant and not necessarily aligned with major shear zones (Fig. 3b).

##### 4.1 Domain A: Diatexite-dominated

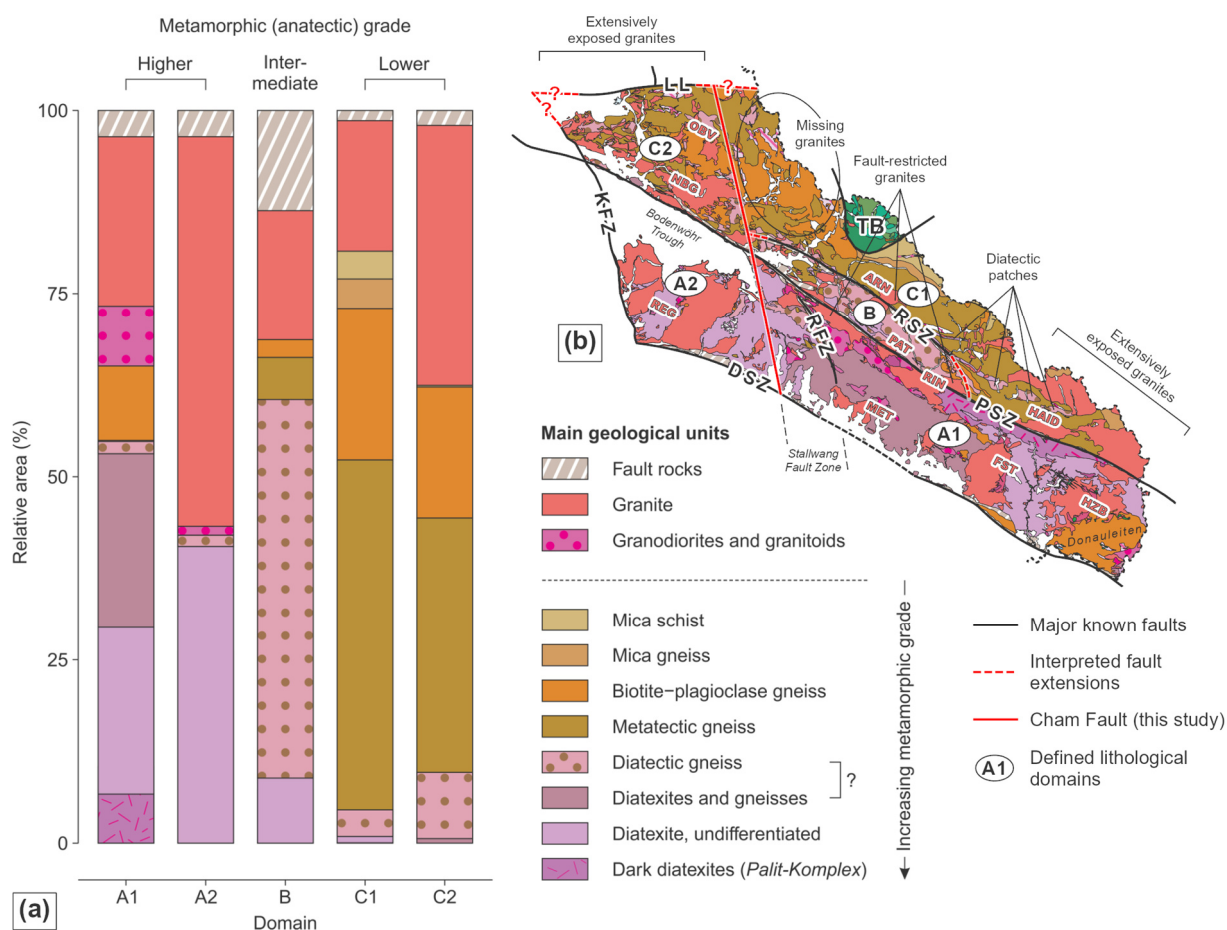
Domain A exposes rocks that have experienced an advanced stage of anatexis, with diatexites forming the predominant rock type (ca. 45 % at the present erosional level, Fig. 3a). In the central part, gneissic rocks are intercalated with diatexites (Fig. 3b). Lower-grade paragneisses are restricted to the so-called “Donau-Serie” in the very southeast of domain A (Daurer, 1976; Fig. 3b). Late Variscan granites in domain A are extensively exposed in the northwest, whereas in the central part, a very limited number of granitic bodies are exposed, which are restricted to the traces of the Pfahl and Danube shear zones

215



220

(e.g., the Metten Massif and the Patersdorf Stock, Fig. 3b). Based on the abundance and distribution of exposed late Variscan granites, a distinct boundary subdivides domain A into domain A2, i.e., the northwestern part with abundant granites, and A1, i.e., the central-southeastern part, where granites are solely exposed along the traces of major fault zones (Fig. 3b). This boundary also defines the southeastern border of the Cretaceous Bodenwöhr Trough and marks the western limit of the ca. 10 km wide, NNW-SSE striking Stallwang Fault Zone (Troll, 1967). Towards the very southeast of domain A1, the abundance of granites gradually increases again and their exposure is not aligned with the Pfahl and Danube shear zones (Fig. 3b).



225

**Figure 3** Statistical and spatial distribution of exposed lithologies. Five domains with characteristic rock inventories can be identified (A1, A2, B, C1, and C2). (a) Stacked bar plots illustrating the relative occupied area of the exposed lithologies in each of the domains (calculations based on geological maps from Teipel et al., 2008 and Galadí-Enríquez et al., 2009b). (b) Detailed geological map of the studied area along the southwestern Bohemian Massif (modified from Teipel et al., 2008; Galadí-Enríquez et al., 2009b). Fault zones: *DSZ* Danube Shear Zone, *KFZ* Keilberg Fault Zone, *LL* Luhe Line, *PSZ* Pfahl Shear Zone, *RSZ* Runding Shear Zone, *RFZ* Rattenberg Fault Zone. Exposed granite bodies: *ARN* Arnbruck Stock, *FST* Fürstenstein Composite Massif, *HAI*D Haidel Massif, *HZB* Hauzenberg Composite Massif, *MET* Metten Massif, *NBG* Neunburg Massif, *OBV* Oberviechtach Stock, *PAT* Patersdorf Stock, *REG* Regensburg Forest Massif, *RIN* Rinchnach Stock; names after Klominský et al. (2010). *TB* Teplá-Barrandian.

230



#### 4.2 Domain B: Diatectic gneiss-dominated

235 Domain B is bounded by the Pfahl and Runding shear zones and is characterized by the exposure of predominantly diatectic  
gneisses (ca. 50 % of the total area) and granites (ca. 20 %, Fig. 3a). Diatectic gneisses are almost entirely restricted to this  
domain. Outside domain B, small patches of diatectic gneisses are aligned subparallel to the Pfahl Shear Zone in the southeast  
of domain C (Fig. 3b). Late Variscan granites in domain B are mainly aligned with the Pfahl and Runding shear zones (Fig.  
3b). A high amount of fault rocks, predominantly mylonites and cataclasites (ca. 15 % of the total area), indicate pervasive  
240 faulting in domain B.

#### 4.3 Domain C: Metatectic gneiss-dominated

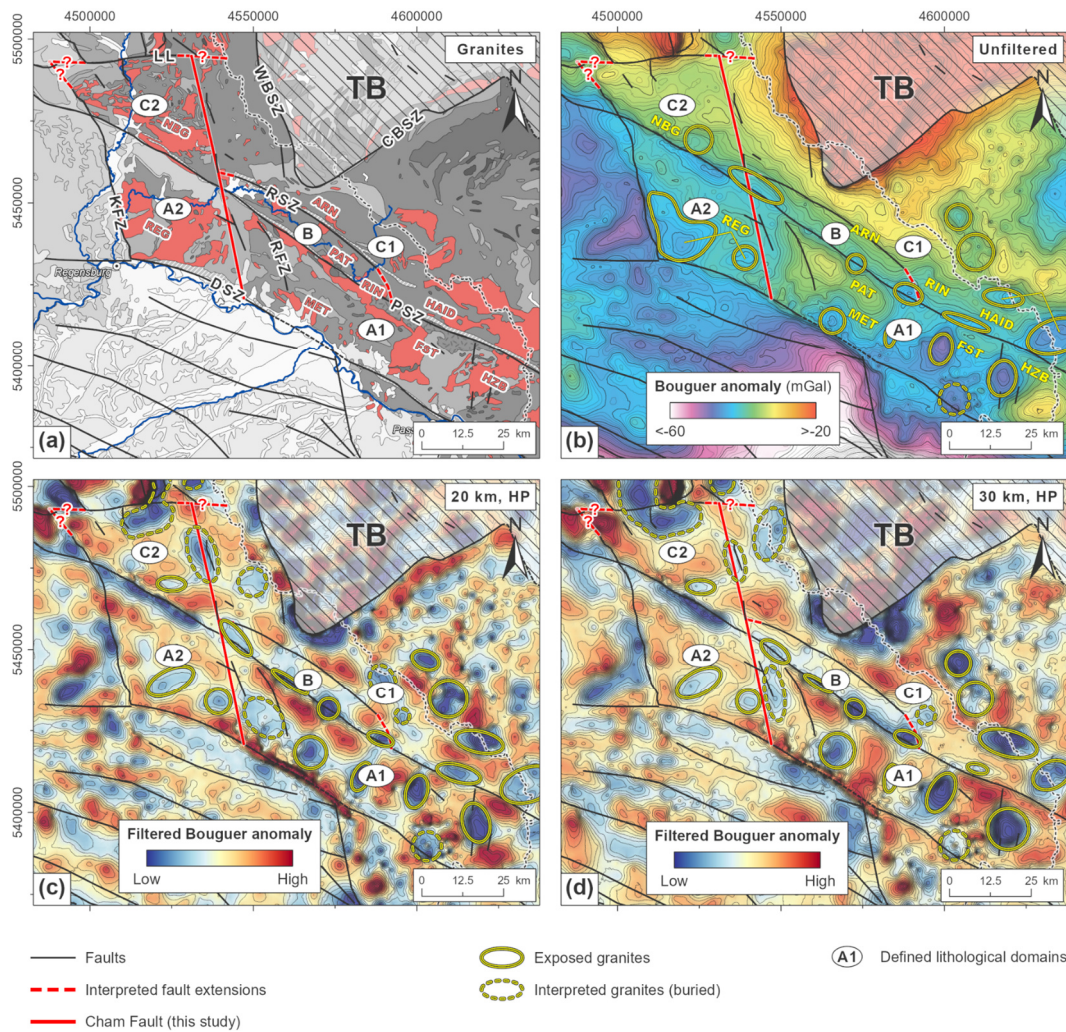
Domain C comprises the area to the northeast of the Pfahl and Runding shear zones and is characterized by the presence of  
intermediate- to high-grade metamorphic rocks. The metamorphic grade in domain C is lower compared to domains A and B  
(Fig. 3b). Tectonostratigraphic units in domain C consist of intermediate-grade biotite-garnet-chlorite schists and higher-grade  
245 biotite-plagioclase gneisses to partially molten metatectic gneisses, the latter representing ca. 50 % of the total area in domain  
C (Fig. 3a). Exposed late Variscan granites in the northwest of domain C terminate towards the center at the previously defined  
boundary subdividing domain A into A1 and A2 (Fig. 3b). We interpret this boundary to represent an important structural  
feature in the study area and call it “Cham Fault”. East of the Cham Fault, in the central part of domain C, granites are solely  
exposed along the Runding Shear Zone (e.g., the Arnbruck Stock, Fig. 3b). Towards the southeast of domain C, exposure of  
250 granites gradually increases, showing a similar pattern as observed in domain A.

### 5 Subsurface distribution of late Variscan granites

The spatial distribution of exposed late Variscan granites with a sharp decrease in abundance across the Cham Fault raises the  
question of whether the granites are generally not present in the central parts of the study area or whether they have not yet  
been exhumed to the surface. Comparing the unfiltered and high-pass filtered Bouguer gravity data with the geological maps  
255 indicates that known granites show circular to semi-circular gravity lows (e.g., Regensburg Forest Massif, Patersdorf Stock,  
Fürstenstein Composite Massif, Hauzenberg Composite Massif, Fig. 4). The densities of exposed granites in the study area  
range from 2640 to 2680 kg/m<sup>3</sup>, whereas the metamorphic country rocks show densities > 2690 kg/m<sup>3</sup> (Table 3). Distinct local  
and circular to semi-circular gravity lows along the western Bohemian Massif that are not associated with exposed granites  
are interpreted as buried granite bodies (e.g., Bott and Smithson, 1967; Behr et al., 1989; Trzebski et al., 1997; Sedlák et al.,  
260 2009; Petkovic, 2014; de Wall et al., 2019). Applying 20 and 30 km high-pass filters confirms the presence of granitic bodies  
(circular and semi-circular gravity lows) at different crustal levels (Figs. 4c and 4d). Some of these subsurface granites trend  
subparallel to major fault zones, similar to their exposed counterparts (Fig. 4a-d). The presence and distribution of buried



granites, as evidenced by filtered gravity anomaly maps, suggest a rather homogenous distribution of granites in the subsurface of the study area (Fig. 4c-d).



265

270

275

**Figure 4** Compilation of unfiltered and filtered gravity data. (a) Gray-scaled geological map of the southwestern Bohemian Massif with exposed late Variscan granites highlighted in red (modified from Freudenberger and Schwerd, 1996; Toloczyki et al., 2006; Teipel et al., 2008; Galadí-Enríquez et al., 2009b). (b) Unfiltered Bouguer anomaly map showing the total gravity signal of the study area and its surroundings (data source: Leibniz-Institut für Angewandte Geophysik, 2010; Skiba, 2011). (c)-(d) High-pass filtered gravity data (20 km and 30 km wavelength, respectively) depicting the upper crustal configuration of the study area. Traces of major fault zones and the interpreted Cham Fault, as well as the locations of exposed and interpreted granite bodies, are shown. Fault zones: *CBSZ* Central Bohemia Shear Zone, *DSZ* Danube Shear Zone, *KFZ* Keilberg Fault Zone, *LL* Luhe Line, *PSZ* Pfahl Shear Zone, *RSZ* Runding Shear Zone, *RFZ* Rattenberg Fault Zone, *WBSZ* West Bohemia Shear Zone. Exposed granite bodies: *ARN* Arnbruck Stock, *FST* Fürstenstein Composite Massif, *HAID* Haidel Massif, *HZB* Hauzenberg Composite Massif, *MET* Metten Massif, *NBG* Neunburg Massif, *PAT* Patersdorf Stock, *REG* Regensburg Forest Massif, *RIN* Rinnach Stock; names after Klominský et al. (2010). *TB* Teplá-Barrandian.



280

The metamorphic rocks surrounding the granites show different gravity signatures. Areas dominated by gneissic rocks generally show less pronounced negative Bouguer anomalies (domain C, Fig. 4b-d). In contrast, rocks of higher metamorphic grades (i.e., diatexites) show more pronounced negative anomalies (domain A, Fig. 4b-d). This relationship can be explained with the density contrasts of the present rock types, with higher-grade metamorphic rocks tending to be less dense compared to lower-grade rocks (Table 3).

**Table 3** Mean densities of granites and metamorphic rocks in the study area [in kg/m<sup>3</sup>]. Equivalent data on metamorphic rocks outside the study area are included. <sup>a</sup>own measurements, <sup>b</sup>Guy et al. (2011), <sup>c</sup>Smithson (1971).

Data type	Rock type	Granite pluton	Mean density (kg/m <sup>3</sup> )
Study area	Granites	Hauzenberg Composite Massif	2650±10 <sup>a</sup>
		Fürstenstein Composite Massif	2680±50 <sup>a</sup>
		Patersdorf Stock	2670±10 <sup>a</sup>
		Metten Massif	2670±10 <sup>a</sup>
		Regensburg Forest Massif	2640±20 <sup>a</sup>
Global data	Metamorphic rocks (approx.)		2690 - 2760 <sup>b</sup>
	Migmatites		2730±60 <sup>c</sup>
	Biotite gneiss and schist		2750±60 <sup>c</sup>
	Mica schist		2800±30 <sup>c</sup>
	Biotite-hornblende gneiss		2860±60 <sup>c</sup>
	Amphibolite		3030±70 <sup>c</sup>

## 6 Topographic analysis

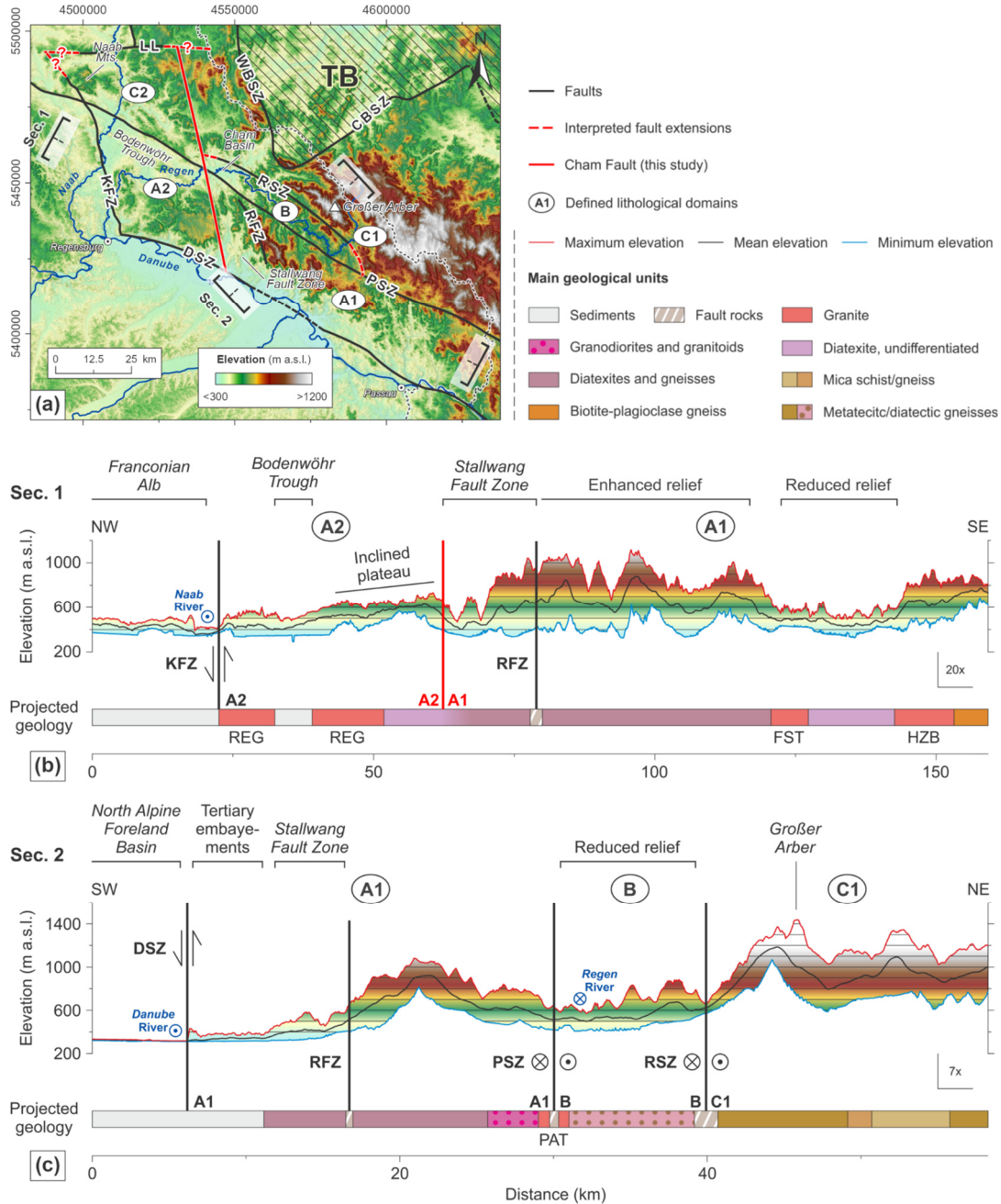
285

In this chapter, we present the morphological analysis results using swath profiles and the mapping of topographic lineaments to confirm and characterize basement domains identified previously based on the spatial distribution of metamorphic rocks and late Variscan granites.

### 6.1 Across- and along-strike variations in topography

290

Two swath profiles illustrate across- and along-strike topographic variations of the southwestern Bohemian Massif (Fig. 5). A mountainous landscape marks the northwestern parts of domain A1 with peaks up to ca. 1000 m a.s.l. (Fig. 5a-b). This elevated area shows an increased abundance of gneissic rocks (Fig. 5b). In contrast, the southeastern parts of domain A1, which is dominated by higher-grade diatexites, show a low-lying landscape with a reduced relief and elevations down to ca. 350 m a.s.l..



295 **Figure 5** (a) DEM depicting the locations of major tectonic structures and swath profiles. (b) Swath profile transecting the study area in a  
 NW-SE direction. (c) Swath profile transecting the study area in a SW-NE direction. Important morphological and tectonic features are  
 indicated. For locations of the profiles, see (a). Fault zones: *CBSZ* Central Bohemia Shear Zone, *DSZ* Danube Shear Zone, *Kfz* Keilberg  
 300 Fault Zone, *LL* Luhe Line, *PSZ* Pfahl Shear Zone, *RSZ* Runding Shear Zone, *RFZ* Rattenberg Fault Zone, *WBSZ* West Bohemia Shear Zone.  
 Exposed granite bodies: *FST* Fürstenstein Composite Massif, *HZB* Hauzenberg Composite Massif, *PAT* Patersdorf Stock, *REG* Regensburg  
 Forest Massif; names after Klominský et al. (2010). *TB* Teplá-Barrandian.



In domain A2, the Variscan basement is predominantly exposed to the south of the Regen River and is characterized by an undulating relief with elevations in between ca. 400 and 750 m a.s.l. (Fig. 5a). The very southeast of that area is marked by a distinctly elevated plateau that gently dips towards the northwest (Figs. 5a-b). To the north of the Regen River, the Mesozoic to Cenozoic sediments of the Bodenwöhr Trough evoke a flat relief (Fig. 5a). The Stallwang Fault Zone, which is defined as the area in between the Cham Fault and the Rattenberg Fault Zone, borders domain A2 to the southeast and is characterized by sub-parallel, NNW-SSE-trending erosional furrows indicating a highly deformed area that favors erosion (Figs. 5a-b). Domain B, with its high-grade metamorphic rocks (diatectic gneisses), shows lower elevations compared to adjacent areas and catches the drainages of its surroundings (Figs. 5a and 5c).

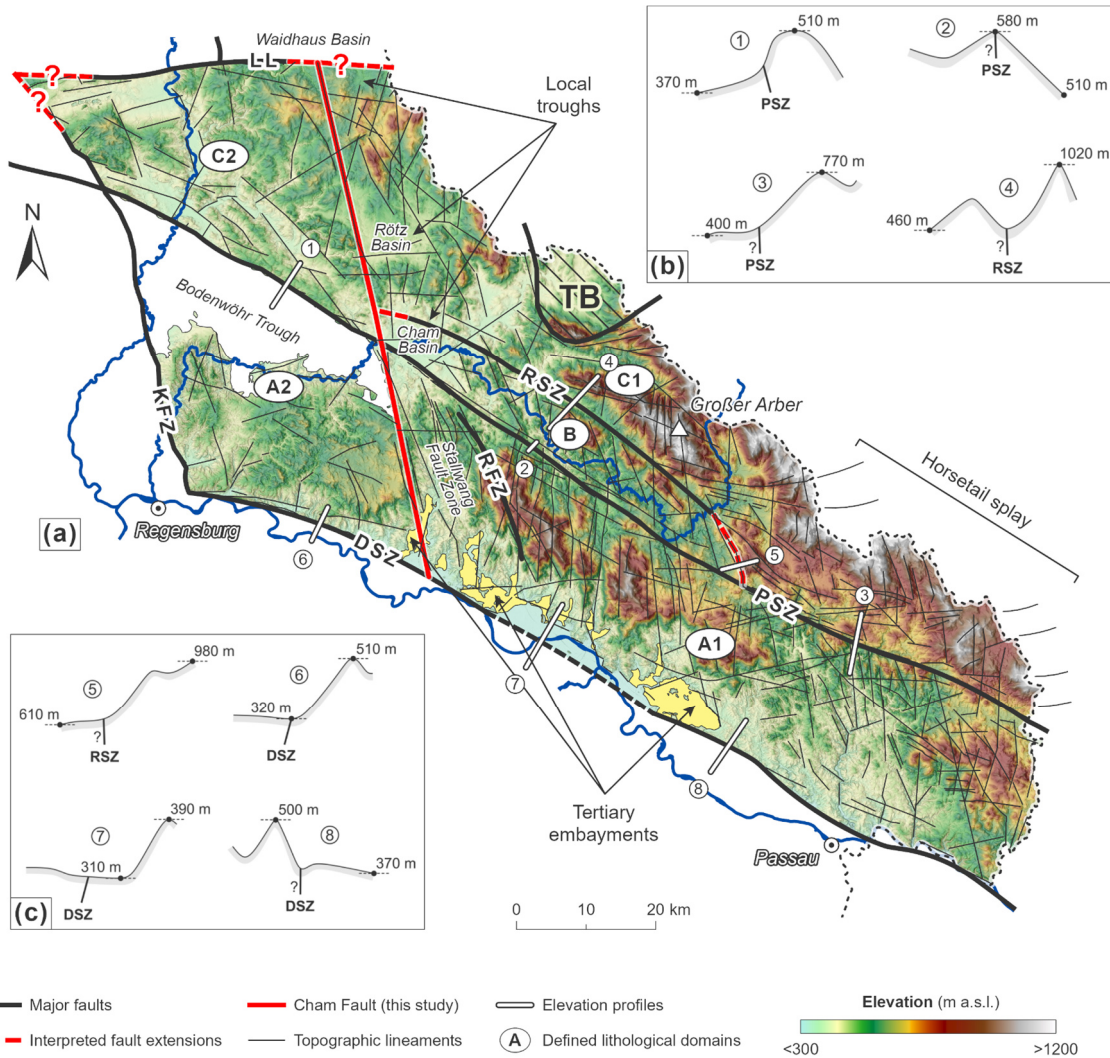
A very diverse topography characterizes the metatectic-dominated area of domain C1, with its eastern part comprising a high-relief mountainous landscape (Figs. 5a and c). In contrast, in the northwest, a heterogeneous landscape with basins (e.g., the Rötz Basin) that are surrounded by peaks up to 900 m a.s.l. high is developed (c.f. Figs. 6a and 7). Domain C2, which is also dominated by metatectic rocks but comprises a much higher number of exposed granites compared to C1, is characterized by low to intermediate elevations of ca. 350 to 750 m a.s.l.. In its center, the landscape is dissected by the broad Naab River valley, draining to the south (Fig. 5a). To the west of the Naab River, the Naab Mountains form a local fault-bounded topographic high (Fig. 5a).

## 6.2 Topographic lineament analysis

In total, 1315 topographic lineaments have been identified in the study area (Fig. 6). Linear river valleys count for ca. 50 %, ridgelines count for ca. 30 %, and sudden breaks in slope count for ca. 10 % of the identified lineaments. The remaining ca. 10 % of the identified lineaments are related to a combination of valleys, ridgelines, and/or slope breaks. Known faults are thereby often associated with distinct lineaments, suggesting a close relationship between tectonic and topographic features.

### 6.2.1 Topographic signatures of major fault zones

Major fault zones are all well-visible in topography (Fig. 6a). The Pfahl Shear Zone is characterized by two different topographic expressions. Along its northwestern and southeastern segments, the shear zone is expressed by pronounced slope breaks (Fig. 6a and profiles 1 and 3 in Fig. 6b). In the northwest, the Pfahl Shear Zone defines the northern border of the Bodenwöhr Trough, whereas its southeastern segment separates a mountainous landscape in the north from a moderate-relief landscape in the south (Fig. 6a). Along its central segment, the Pfahl Shear Zone forms a narrow but distinct morphological ridge (Fig. 6b, profile 2). This morphological ridge is attributed to the pervasive quartz mineralization along the Pfahl Shear Zone (Priehäusser, 1961).



330 **Figure 6** Lineament inventory of the study area. (a) DEM depicting lineaments traces, major fault zones, and the interpreted Cham Fault. The location of important topographic features like troughs and tertiary embayments are outlined. Note that only higher-order lineaments are shown to maintain clarity. (b)-(c) Elevation profiles across the different topographic segments of the Pfahl, Runding, and Danube shear zones. Question marks indicate unknown dip-directions of the associated faults. Fault zones: *DSZ* Danube Shear Zone, *KFZ* Keilberg Fault Zone, *LL* Luhe Line, *PSZ* Pfahl Shear Zone, *RSZ* Runding Shear Zone, *RFZ* Rattenberg Fault Zone. *TB* Teplá-Barrandian.

335 The Runding Shear Zone is predominantly characterized by deeply incised river valleys (Fig. 6a and profile 4 in Fig. 6b). To the northwest, the Runding Shear Zone terminates against the Cham Fault and borders the Cham Basin to the north (Fig. 6a). This contrasts to the southeast, where the Runding Shear Zone is expressed as a distinct slope break terminating against the Pfahl Shear Zone (Fig. 6a and profile 5 in Fig. 6c). Here, elevations of up to 1000 m a.s.l. occur to the northeast of the Runding Shear Zone, whereas generally lower elevations of less than 650 m a.s.l. prevail to the southwest. Interestingly, our data also





340 provide evidence for the presence of several lineaments splitting off the Runding Shear Zone towards the east and southeast. These lineaments rotate from an overall NW-SE into an E-W orientation, indicating the presence of a horsetail splay originating from the terminating Runding Shear Zone (Fig. 6a).

The Danube Shear Zone and Keilberg Fault Zone show distinct slope breaks in topography (Fig. 6a). In the case of the Danube Shear Zone, however, this slope break is not expressed uniformly along-strike. Along the northwestern segment of the Danube Shear Zone, the slope break occurs very abruptly (Fig. 6a and profile 6 in Fig. 6c), whereas the central segment is largely buried beneath the Cenozoic sediments of the North Alpine Foreland Basin (profile 7 in Fig. 6c). At this location, the topography is very irregular, with numerous embayments of Cenozoic sediments occurring across the Danube Shear Zone and reaching far into the crystalline basement in the northeast (Fig. 6a). The boundary between the topographically well-expressed northwestern and the sediment-covered central segment of the Danube Shear Zone is defined by the Cham Fault (Fig. 6a). The southeasternmost segment of the Danube Shear Zone (locally called Aicha-Halser-Nebenpfahl) deviates from the course of the Danube River and separates a local basement high in the south from domain A1 in the north (Fig. 1b and profile 8 in Fig. 6c).

The Cham Fault is also characterized by a well-defined topographic lineament (Fig. 7). The fault separates the elevated plateau and the sedimentary fill of the Bodenwöhr Trough in the northwest (domain A2) from the incised landscape of the Stallwang Fault Zone in the southeast (domain A1). The central part of the Cham Fault consists of at least two main segments cross-cutting the Pfahl Shear Zone and bordering the Cham Basin to the west (Fig. 7). At this location, the Runding Shear Zone terminates against the Cham Fault. In the north, the Cham Fault separates the Rötz Basin from an elevated and deeply incised landscape in the eastern part of domain C2. Here, the fault is manifested as a single, distinct lineament, which can be traced at least up to the inferred eastern extension of the Luhe Line in the north (Fig. 7).

### 360 **6.2.2 Statistical analysis of topographic lineaments**

Mapped lineaments mainly strike (I) NW-SE/WNW-ESE sub-parallel to the Pfahl, Danube, and Runding shear zones, and (II) NNW-SSE/N-S (Fig. 8a). Lineaments striking NNW-SSE/N-S are oriented subparallel to the Cham Fault and the Keilberg Fault Zone and are especially abundant within domain A1, where subparallel river valleys are deeply incised into the mountainous landscape (Figs. 5b and 6). A third, subordinate ca. E-W striking direction observed in the lineament inventory is mainly related to the lineaments forming the proposed horsetail splay in the southeast of domain C1 (Figs. 6 and 8a).

Mapped faults dominantly strike NNW-SSE/N-S, while the major basement domain bounding Pfahl, Danube, and Runding shear zones strike NW-SE/WNW-ESE and only represent a minor peak in the rose diagram (Fig. 8b). This observation can be related to the technical representation of major fault zones in the analyzed geological maps, being expressed as wide zones of fault rocks rather than single lines (Teipel et al., 2008; Galadí-Enríquez et al., 2009b). Therefore, individual structural elements of the shear zones could not be included in the directional statistical analysis, which slightly biases the relative proportions of fault orientations.

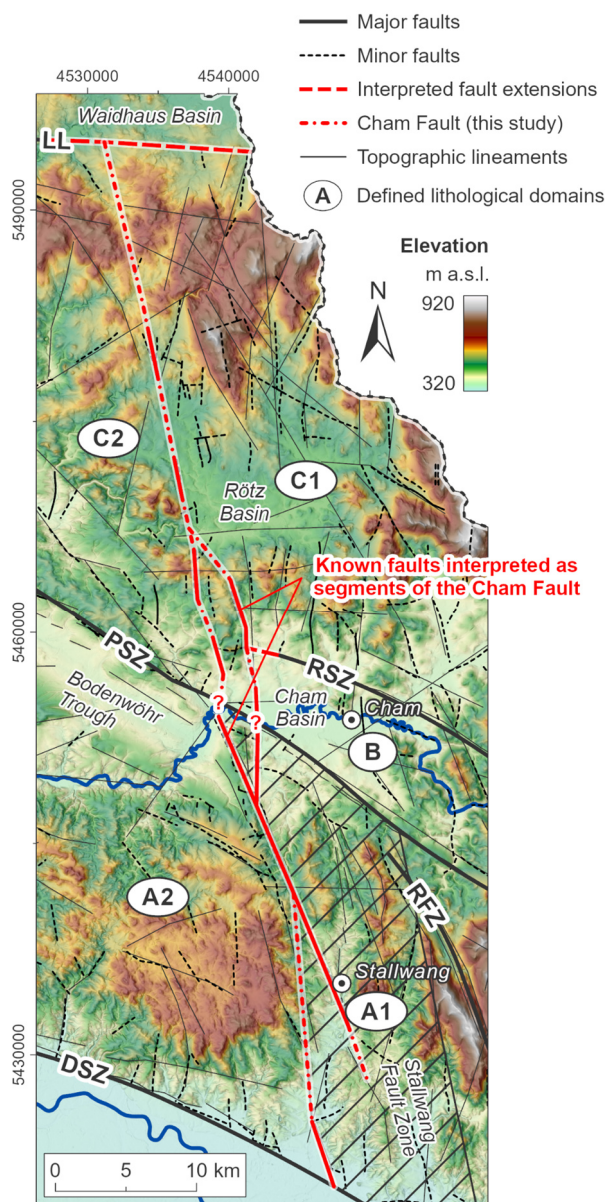


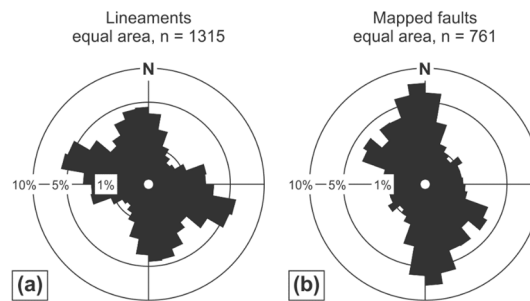
**Figure 7** Detailed map of the Cham Fault as inferred from the DEM. Several known faults from the geological map are interpreted as segments of the Cham Fault. Note the uncertainty in the location of the southernmost part of the fault, which is due to enhanced erosion along the Stallwang Fault Zone. Fault zones: *DSZ* Danube Shear Zone, *LL* Luhe Line, *PSZ* Pfahl Shear Zone, *RSZ* Runding Shear Zone, *RFZ* Rattenberg Fault Zone.

375

Domains A1, A2, and C1 show distinct peaks in both NW-SE/WNW-ESE and NNW-SSE/N-S directions, similar to the overall trends of lineaments and faults in the study area (Figs. 8 and 9). In contrast, domain B only shows a subordinate NW-SE to WNW-ESE oriented peak. Here, most of the lineaments are oriented NNW-SSE/N-S. Domain C2 shows a unique orientation

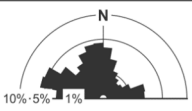







380 pattern, with a distinct peak in the NW-SE/WNW-ESE directions, whereas N-S lineaments are almost entirely missing in this area (Fig. 9).



**Figure 8** Rose diagrams of (a) mapped lineaments and (b) faults from geological maps. The diagrams have been length-weighted to account for great length variations.

385 The lineament densities also vary across the study area. Lineament densities to the west of the Cham Fault (domains A2 and C2, ca. 0.57 and 0.76 km/km<sup>2</sup>, respectively) are lower in comparison to areas east of the Cham Fault (domains A1, B, and C1, between ca. 0.84 and 1.05 km/km<sup>2</sup>). Domain B shows the highest density of lineaments with ca. 1.05 km/km<sup>2</sup> (Fig. 9).

Entire dataset	Domain A1	Domain A2
		
n = 1315	n = 515	n = 179
Mean R = 0.32	Mean R = 0.26	Mean R = 0.19
Density = 0.75 km/km <sup>2</sup>	Density = 0.97 km/km <sup>2</sup>	Density = 0.76 km/km <sup>2</sup>
Domain B	Domain C1	Domain C2
		
n = 69	n = 250	n = 119
Mean R = 0.33	Mean R = 0.20	Mean R = 0.35
Density = 1.05 km/km <sup>2</sup>	Density = 0.84 km/km <sup>2</sup>	Density = 0.57 km/km <sup>2</sup>

390 **Figure 9** Statistical analysis of the mapped lineaments carried out for the entire dataset and separately for each of the five defined domains. The analysis includes rose diagrams (length-weighted, bin size = 10°), as well as calculations regarding the statistical scatter (mean resultant) and the mean spatial density of the lineaments. The mean resultant (*Mean R*) is a measure of dispersion analogous to the variance but expressed in the opposite sense. Lower values indicate a more dispersed distribution or the presence of different individual peaks, whereas higher values indicate that the observations are tightly bunched together (Davis, 2002). Only lineaments outside of a 2 km buffer along the domain boundaries were considered in the analysis to avoid biases related to the trends and lengths of the major fault zones and associated lineaments. For comparison, the rose diagram of all lineaments in the entire area is shown (not buffered). Note that the Bodenwöhr Trough in domain A2 and the Cham Basin in domain B (c.f., Fig. 5) have been excluded from the analysis due to their sedimentary infill.

395



## 7 Observations from low-temperature thermochronological data in the study area

We compiled thermochronological data from the literature that were obtained on apatite and zircon reflecting the low-temperature history of the study area (Fig. 10). On either side of the Cham Fault, two Zircon Fission Track (ZFT) data points, located ca. 2 km apart (Fig. 10b), record an apparent age gap of ca. 45 Myrs (ca. 260 Ma and 215 Ma, respectively, data from C.W. Naeser in Gebauer, 1984 and Wagner et al., 1997). Similar ages of ca. 250 Ma have been reported from a quarry to the south of the Luhe Line (northeastern part of domain C2) and a sample located in the central-eastern part of domain A2 (data from C.W. Naeser in Gebauer, 1984). In contrast, younger apparent ZFT ages of ca. 215 Ma are known from the Passau Forest, located close to the southern end of domain A1 outside the study area, and from the area adjacent to the Teplá-Barrandian Unit (Domain C1, data from C.W. Naeser in Gebauer, 1984).

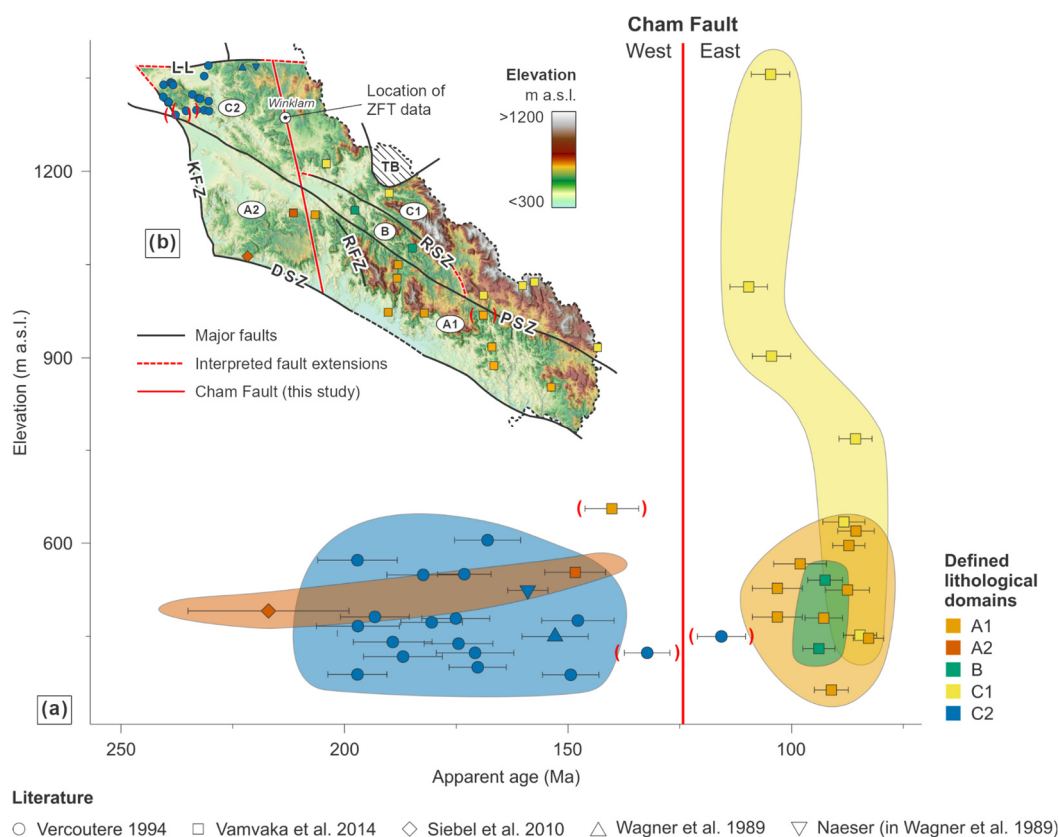


**Figure 10** Compilation of Apatite Fission Track (AFT) data from the literature (Wagner et al., 1989; Vercoutere, 1994; Siebel et al., 2010; Vamvaka et al., 2014). (a) Age-elevation plot color-coded according to the sample's domain affiliation. Note that the Cham Fault separates two distinct clusters of AFT apparent ages. Calculation of the sample altitudes has been done based on a DEM with a 1-meter horizontal resolution using the sample location coordinates. (b) DEM depicting the locations of the samples shown in (a). Note that the village of Winklarn depicts the sample locations of published ZFT data, with one sample located at each side of the Cham Fault within a 2 km distance (see text for details). Fault zones: *DSZ* Danube Shear Zone, *KFZ* Keilberg Fault Zone, *LL* Luhe Line, *PSZ* Pfahl Shear Zone, *RSZ* Runding Shear Zone, *RFZ* Rattenberg Fault Zone. *TB* Teplá-Barrandian.



415 Low-temperature Apatite Fission Track (AFT) data also show significant spatial differences in apparent ages across the Cham  
Fault, even among samples obtained at similar altitudes (Wagner et al., 1989; Vercoutere, 1994; Siebel et al., 2010; Vamvaka  
et al., 2014; Fig. 10a). An apparent age gap of ca. 40 to 50 Myrs is recorded between two clusters separated by the newly  
defined Cham Fault. In the area to the northwest of the Cham Fault (domains A2 and C2), AFT apparent ages mainly cluster  
between ca. 150 and 200 Ma, whereas to the southeast of the fault (domains A1, B, and C1), most AFT data record apparent  
ages below ca. 100 Ma (Fig. 10a). No significant correlation between sampling elevation and ages is observed in the compiled  
420 AFT dataset. In addition, the data do not show a clear age gap across the Pfahl and Runding shear zones.

## 8 Discussion

By analyzing Bouguer gravity anomaly, topographic, and geological data, we identified three main basement domains in the  
southwestern Bohemian Massif. These domains are interpreted as individual basement blocks that were differentially uplifted  
during and after the late Paleozoic Variscan Orogeny. Furthermore, the heterogeneous distribution of exposed granites and  
425 available thermochronological data show a second segmentation by the previously unknown crustal-scale Cham Fault. Below  
we discuss the timing and succession of the observed block segmentation and its implications for the tectonic framework along  
the southwestern Bohemian Massif.

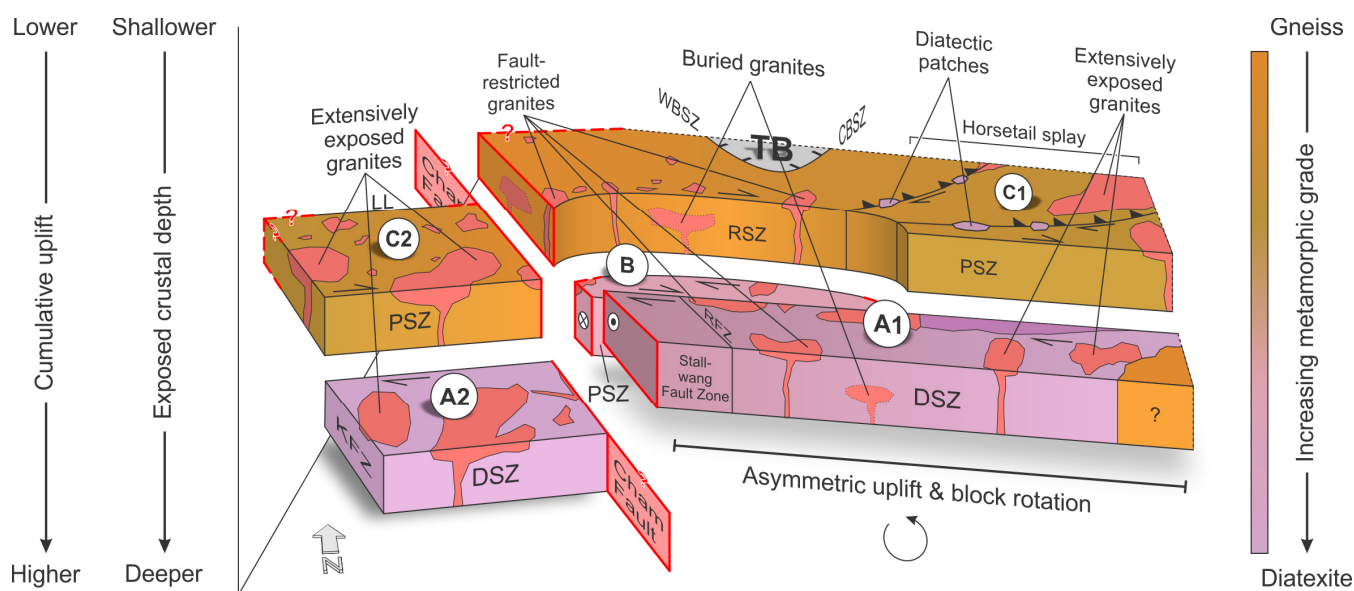
### 8.1 Lithological evidence for block segmentation

The observed metamorphic units across the study area are interpreted as being part of a genetic sequence of thermally over-  
430 printed rocks, starting from intermediate-grade biotite-garnet-chlorite schists adjacent to the southern tip of the Teplá-Barran-  
dian Unit over high-grade biotite-plagioclase gneisses to partially molten (metatectic) gneisses in the southeast of domain C  
(Blümel, 1972). Consequently, the diatexites of domain A can be considered as successors in this sequence, where advanced  
partial melting of the metatectic precessors has led to the formation of nebulitic or schlieren textures (e.g., Wimmenauer and  
Bryhni, 2007; Chen and Grapes, 2007). The metamorphic rocks of domain B are interpreted to have formed during an inter-  
435 mediate stage of anatexis compared to domains A and C. A strong correlation between metamorphic grades and rock densities  
is observed, resulting in distinct variations of Bouguer anomalies between the identified domains. Higher grade, diatectic  
domains thereby show more pronounced negative Bouguer anomalies compared to lower-grade, gneissic domains. Based on  
this relationship, domain B likely comprises rocks with a higher mean metamorphic grade (“diatectic gneisses”) compared to  
the central part of domain A (“diatexites and gneisses”), important information that is not directly assessable from recent  
440 geological maps (Fig. 3). The distribution of diatectic gneisses in domain B and the presence of a distinct topographic lineament  
suggests a previously unknown extension of the southeastern tip of the Runding Shear Zone towards the south, terminating  
against the Pfahl Shear Zone (Figs. 3 and 6).



445

We suggest differential uplift and exhumation of the crust along distinct, basement block-bounding fault zones as a cause of the observed differences in metamorphic grades (Fig. 11). The generally higher metamorphic grades in domain A indicate a higher total amount of uplift southwest of the Pfahl Shear Zone. In contrast, domain C, dominated by metatectic gneisses, is interpreted to have experienced a lower amount of uplift. The intermediate grade metamorphic rocks in domain B indicate a lower amount of uplift compared to domain A2 and the southeastern part of domain A1 but a higher amount of uplift compared to domain C and the northwestern part of domain A1.



450

**Figure 11** Proposed three-dimensional block model of the southwestern Bohemian Massif. Distinct fault zones separate blocks of different lithological, gravity, and topographic characters, pointing to the exposure of different crustal levels and, thus, to varying amounts of cumulative uplift, the latter increasing from domain C towards domain A. To the southeast of the Cham Fault, asymmetric uplift has led to the tilting of the entire area towards the northwest. Note that the relative depth in the model shows the exposed crustal level, which is vice versa to the tectonic uplift and tilt. Fault zones: *CBSZ* Central Bohemia Shear Zone, *DSZ* Danube Shear Zone, *KFZ* Keilberg Fault Zone, *LL* Luhe Line, *PSZ* Pfahl Shear Zone, *RSZ* Runding Shear Zone, *RFZ* Rattenberg Fault Zone, *WBSZ* West Bohemia Shear Zone. *TB* Teplá-Barrandian.

455

460

A sharp contrast in the spatial distribution of exposed late Variscan granites from the northwest to the southeast is used as evidence for another level of segmentation along the Cham Fault. This fault separates areas exposing shallower crustal levels with less abundant granite exposures in the southeast (domains A1, B, and C1) from areas exposing deeper crustal levels and a higher number of granites in the northwest (domains A2 and C2, Fig. 3). From the Cham Fault to the southeast, granite exposure gradually increases. This observation is interpreted as a counterclockwise block rotation to the east of the Cham Fault (domains A1, B, and C1, Fig. 11). This rotation resulted in the exposure of deeper crustal levels in the very southeast of the study area, where both metamorphic grades and the amount of exposed late Variscan granites are similar to those observed in



domains A2 and C2, respectively (e.g., diatexites in between the Fürstenstein and Hauzenberg composite massifs, Figs. 3 and 11).

465 Exposed late Variscan granites in the center of the study area are aligned with the Pfahl, Runding, and Danube shear zones. These tectonic structures appear to have guided magma ascent in this area, acting as low-pressure zones enabling magma transport to upper crustal levels as it is also observed, e.g., in the Alps and northeastern Brazil (Rosenberg, 2004; Weinberg et al., 2004). In the deeper subsurface, a nearly uniform distribution of granites is shown by the filtered Bouguer gravity anomaly data (Fig. 4). Consequently, the (I) limited exposure of granites, (II) exclusive exposure of fault-related granites, and (III) 470 preservation of gneissic rocks within the diatectic frame to the south of the Pfahl Shear Zone (in between the Patersdorf Stock and the Metten Massif, Fig. 3) can be explained by block rotation and differential uplift.

## 8.2 Topographic evidence for block segmentation

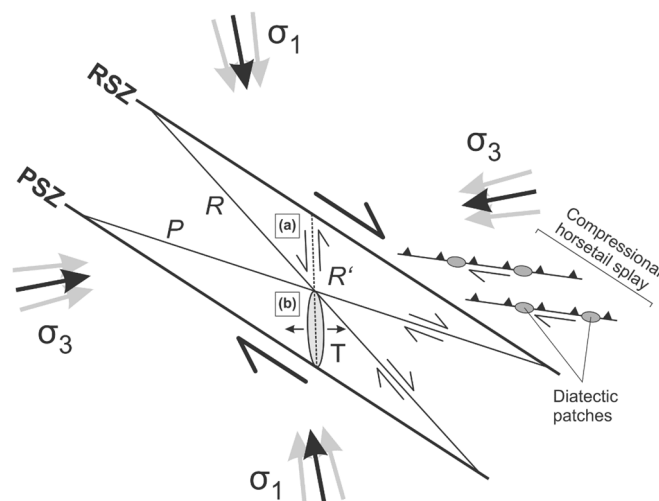
The topographic analysis highlights a close relationship between metamorphic grades and topographic relief, with higher- 475 grade metamorphic rocks being more prone to erosion compared to lower-grade metamorphic rocks (Fig. 5). This relationship supports our interpretation of domain B comprising higher-grade metamorphic rocks compared to the central part of domain A (i.e., the northwestern part of domain A1), as it shows distinctly lower elevations compared to adjacent areas and thus catches the drainages of its surroundings.

Lineaments mapped based on topographic data along the southwestern Bohemian Massif greatly exceed both numbers and 480 lengths of faults known from geological maps. This suggests the presence of a considerable number of yet unidentified faults or fault segments. From the statistical analysis, two main lineament directions (I) NNW-SSE/N-S and (II) NW-SE/WNW-ESE have been identified (Fig. 8). These directions correspond to faults known from geological maps and are in line with the prevailing trend of the large, late-Variscan fault zones, e.g., the Pfahl Shear Zone, Danube Shear Zone, and Keilberg Fault Zone. Therefore, a similar origin regarding timing and tectonic framework can be assumed for most of the mapped structures. 485 A third, ca. E-W oriented direction in the lineament inventory originates from the proposed horsetail splay located in the southeast of the study area. Such an E-W orientation has not yet been observed in mapped faults.

The tectonic configuration of the southwestern Bohemian Massif during the late stages of the Variscan Orogeny is interpreted as a conjugate shear system related to N-NNW directed shortening (Wallbrecher et al., 1991; Brandmayr et al., 1995; Galadí- 490 Enríquez et al., 2010). Under this tectonic regime, a Riedel-type fault interaction likely initiated the observed lineament patterns (Zeitlhöfler, 2007; Fig. 12). In such a model, NW-SE to NNW-SSE striking lineaments would represent synthetic strike-slip faults with a right-lateral sense of motion (“Riedel-Shears”). In contrast, NNW-SSE to N-S striking lineaments reflect either antithetic strike-slip faults with a left-lateral sense of shearing (“R’-Shears”) or, depending on the precise stress field orientation, extensional fractures (“tension gashes”, Fig. 12). Our results confirm a Riedel-type fault interaction in domain B, which is tightly bracketed by the Pfahl and Runding shear zones and shows by far the highest density of lineaments and fault



495 rocks among the identified domains (Figs. 9 and 3). The identified lineaments that split off the Runding Shear Zone in the  
southeastern part of domain C are interpreted as fault branches forming a compressional horsetail splay (Figs. 11 and 12). This  
horsetail splay could also be responsible for the occurrence of diatectic patches arranged in a chain-like pattern in domain C  
(Figs. 3, 11, and 12). On a regional scale, the general structural configuration is also interpreted to reflect Riedel-type fault  
interactions, which most likely initiated during late to post-Variscan wrench tectonics (Peterek et al., 1996; Peterek et al., 1997;  
500 Zeitlhöfler, 2007).



510 **Figure 12** Interpreted tectonic framework in domain B based on the orientations of mapped topographic lineaments (modified and extended  
after Zeitlhöfler, 2007). Depending on the stress field orientation, NNW-SSE to N-S striking lineaments were formed either as (a) antithetic  
strike-slip faults with a left-lateral sense of motion ( $R'$ ) or (b) as extensional fractures ( $T$ ). Fault zones: *PSZ* Pfahl Shear Zone, *RSZ* Runding  
505 Shear Zone.

### 8.3 Thermochronological evidence for block faulting

Low-temperature thermochronological ages in the study area range from late Triassic to late Cretaceous and thus clearly post-  
date tectonothermal processes related to the late Paleozoic Variscan Orogeny. The spatial distribution of compiled data points  
shows that the newly identified Cham Fault separates two distinct clusters of Fission-Track ages. AFT data obtained to the  
510 northwest of the fault are thought to represent post-Variscan cooling ages that were partially reset during Mesozoic burial and  
re-heating (Vercoutere, 1994; Wagner et al., 1989; Hejl et al., 1997; Vamvaka et al., 2014). In contrast, most of the AFT data  
southeast of the Cham Fault suggest ongoing, slow exhumation during the Jurassic and Cretaceous, although slight re-heating  
might also have occurred (Vamvaka et al., 2014).

Regardless of the true nature of the compiled FT ages (i.e., cooling ages or mixed ages), the fact that samples located on both  
515 sides of the Cham Fault within a distance of only a few kilometers show very different apparent ages of 260 and 215 Ma  
suggests that differential block movements provide the most plausible explanation for contrasting thermal histories across the





520 Cham Fault. Our interpretation is in line with Gebauer (1984), who explained an observed gap in two ZFT ages next to the village of Winklarn as a result of 2.5 to 3 km vertical displacement along a distinct tectonic structure (i.e., the Cham Fault) during the Triassic. In contrast to the Cham Fault, the Pfahl and Runding shear zones do not delimit areas of different thermo-chronological histories. Large, differential tectonic movements across these faults were probably absent at least in post-Cretaceous times (Vamvaka et al., 2014).

#### 8.4 Relative timing and succession of block segmentation events

525 ZFT data indicate unroofing of the western Bohemian Massif during Permian and Triassic times (Hejl et al., 1997). This is supported by Permian syn-tectonic sedimentation in the Donaustauf Basin bounded by the northwestern segment of the Danube Shear Zone (Siebel et al., 2010). K-Ar and Rb-Sr illite ages thereby bracket uplift and erosion of the Variscan basement and tectonic extension to a period prior to 255-266 Ma (Siebel et al., 2010).

530 From the lithological and thermochronological data, at least two phases of post-Variscan fault movement and basement block segmentation along the southwestern Bohemian Massif can be inferred. (I) Vertical displacements along the major NW-SE striking Pfahl, Danube, and Runding shear zones, segmenting the area into NW-SE trending blocks of different metamorphic grades (“Pfahl Phase”), and (II) tectonic movements along the Cham Fault, being responsible for further block segmentation and counterclockwise block rotation (“Cham Phase”, Fig. 11). Contrasting cross-cutting relationships between the major faults and the late Variscan granites, however, provide a challenge to reconstruct the exact timing of these two phases:

535 (I) Pfahl Phase: The Pfahl and the Runding shear zones cross-cut (Patersdorf Stock ca. 323 Ma: Siebel et al., 2006a and Arnbruck Stock ca. 325 Ma: Siebel et al., 2008) or, in some places, truncate granites (Rinchnach Stock ca. 320-329 Ma: Siebel et al., 2006a and Haidel Massif ca. 323 Ma: Siebel et al., 2008; Table 1; Fig. 3). Together with a distinct mylonite zone within the Patersdorf Stock, this indicates an activity along the Pfahl and Runding shear zones post-dating the emplacement of late Variscan granites (Siebel et al., 2006a; Büttner, 2007). This is further supported by quartz mineralizations within the mylonite zone (“Pfahl Quartz”) of the Pfahl Shear Zone, indicating a Triassic reactivation of the shear zone (Horn et al., 1986). In contrast, numerous granites appear to have utilized the NW-SE striking fault zones for their ascent, indicating that the faults already existed during granite emplacement. Additionally, there is indication that post-Variscan faulting and shear zone formation in the uplifted basement follows pre-existing structures formed in the deeper continental crust in a late stage of the Variscan Orogeny prior to granite emplacement. Linear intrusions of I-type granodiorites containing abundant mafic enclaves (“Palit-Komplex”, Fig. 545 3) at 334 Ma (Siebel et al., 2005) delineate weak zones in the deeper crust that have been overprinted by the Pfahl shear zone during and after the basement uplift.



(II) Cham Phase: The restricted exposure of late-orogenic granites to the northwest (most likely the hanging-wall) of the Cham Fault suggests post-magmatic faulting as the fault sharply cuts the granite inventory (Fig. 3). Erosional products of late-orogenic granites deposited in adjacent Permian basins indicate rapid exhumation and erosion during the Cham Phase shortly after Upper Carboniferous to early Permian granite emplacement (Mielke, 1993; Galadí-Enríquez et al., 2009a).

As it becomes apparent from the timing indicators for fault activity and block segmentation mentioned above, the Pfahl Phase cannot be considered as a single event but rather as a series of events, which, in total, resulted in a higher total amount of uplift towards the southeast of the Pfahl Shear Zone (domain A). Total vertical uplift during the Pfahl Phase must have amounted to less than the mean 14-18 km emplacement depth of the granites (Table 1). Otherwise, a homogeneous distribution of granites, as observed in domains A2 and C2 and in the deeper subsurface, would be expected across the surface of the entire study area (Fig. 4). In contrast, the Cham Phase is considered as post-magmatic and involved higher amounts of uplift in the northwest (domains A2 and C2) and, likely due to block rotation, in the southeast of the study area. This segmentation phase resulted in the area-wide exposure of granite bodies at the Earth's surface, with total uplift and denudation during both segmentation phases (i.e., the Pfahl and Cham phases) exceeding the estimated granite emplacement depths of 14-18 km (Table 1).

## 9 Conclusions

Our integrated study using gravity anomaly and topographic data provides insights into the crustal architecture of the southwestern Bohemian Massif. Domains of different metamorphic grades and/or exposed granite inventories are interpreted as individual crustal blocks that are bordered by distinct tectonic structures. With the Cham Fault, we introduce a previously unknown NNW-SSE striking tectonic structure that is of similar importance to other major fault zones, such as the Pfahl and Danube shear zones. We propose a model of differential uplift and block rotation that led to the juxtaposition of contrasting lithological domains. Increasing amounts of uplift evoked the exposure of deeper crustal levels, as evidenced by the presence of higher metamorphic grades and a higher percentage of granite bodies at the surface. Gravity anomaly filterings thereby indicate a rather homogeneous distribution of granites in the subsurface. This observation contrasts with the heterogeneous exposure of granites at the surface, suggesting that an important phase of segmentation and differential uplift must have occurred after granite emplacement. A post-Variscan activity of the Cham Fault is evidenced by abrupt changes of apparent ZFT and AFT ages across the tectonic structure. The fact that the Cham Fault also forms tectonic boundaries of Cretaceous to Cenozoic geological features, such as the Bodenwöhr Trough, implies that it played a significant role in the tectonic evolution of the southwestern Bohemian Massif even during the younger geological past.

Our model of block segmentation and differential uplift along the southwestern Bohemian Massif emphasizes the significance of vertical displacements along distinct tectonic structures to explain the observed complex lithological configuration in the



580 study area. The example of the newly discovered Cham Fault thereby suggests that potentially several more yet unidentified  
tectonic structures might exist in that area. To precisely reconstruct the timing and succession of block segmentation events  
along the discussed faults and to quantify the amounts of uplift of the five outlined basement blocks, however, additional data  
on granite intrusion depths, P-T metamorphic conditions, and thermochronology are needed.

585 **Data availability.** The high-resolution topographic data used in this study are available by request at the Bavarian Agency for  
Digitisation, High-Speed Internet and Surveying. The Bouguer anomaly data are provided by the Leibniz Institute for Applied  
Geophysics (LIAG).

590 **Author contribution.** AE, HF, WB, and HS designed the study. AE prepared the manuscript and performed the analysis of  
the topographic, filtered gravity, granite density, and literature data. HF carried out the filtering of the gravity data and super-  
vised the study. HS and HdW supervised and acquired the financial support for the project leading to this publication. GG  
provided the gravity data and supported their interpretation. All authors contributed to the reviewing of the manuscript and the  
595 discussion of the results.

**Competing interests.** The authors declare that they have no conflict of interest.

600 **Acknowledgements.** This research was part of the project “Lithologische und strukturelle Untersuchungen im ostbayerischen  
Grundgebirge“, which was funded within the scope of the project initiative “Bodenatlas Bayern” by the Government of Bavaria  
with co-funding of the European Union (EFRE-Programm Bayern 2014-2020). We would like to thank Caroline Vercoutere  
and Agni Vamvaka for providing details on their AFT analyses and Johann Rohrmüller, Timo Spörlein, Volker Friedlein,  
605 Melanie Meyer (all LfU Bayern), and Tobias Stephan for fruitful discussions.



## References

- Asch, K.: IGME 5000: 1:5 Million International Geological Map of Europe and Adjacent Areas, Bundesanstalt für Geowissenschaften und Rohstoffe, Hannover, 2005.
- 610 Barrier, E., Chamot-Rooke, N., and Giordano, G.: Geodynamic map of the Mediterranean, 2004.
- Bauberger, W. and Cramer, P. (Eds.): Erl. Geol. Kt. Bayern 1:25.000, Bl. 6838 Regenstauf, München, 1961.
- Beer, W. W.: Die strukturelle Entwicklung der Metamorphite des Bayerischen Waldes., PhD thesis, Mathematisch-Naturwissenschaftliche Fakultät, Georg-August-Universität Göttingen, Göttingen, 1981.
- Behr, H.-J., Große, S., Heinrichs, T., and Wolf, U.: A Reinterpretation of the Gravity Field in the Surroundings of the KTB  
615 Drill Site - Implications for Granite Plutonism and Terrane Tectonics in the Variscan, in: The German continental deep drilling program (KTB): Site selection studies in the Oberpfalz and Schwarzwald, edited by: Emmermann, R., Springer, Berlin, Heidelberg, New York, London, Paris, Tokyo, Hong Kong, 501-525, 1989.
- Blümel, P.: Die Analyse von Kristallisation und Deformation einer metamorphen Zonenfolge im Moldanubikum von Lam-Bodenmais, N. Jb. Miner. Abh., 118, 74–96, 1972.
- 620 Bott, M. H. P. and Smithson, S. B.: Gravity Investigations of Subsurface Shape and Mass Distributions of Granite Batholiths, Geol. Soc. Am. Bull., 78, 859, [https://doi.org/10.1130/0016-7606\(1967\)78\[859:GIOSSA\]2.0.CO;2](https://doi.org/10.1130/0016-7606(1967)78[859:GIOSSA]2.0.CO;2), 1967.
- Brandmayr, M., Dallmeyer, R. D., Handler, R., and Wallbrecher, E.: Conjugate shear zones in the Southern Bohemian Massif (Austria): implications for Variscan and Alpine tectonothermal activity, Tectonophysics, 248, 97–116, [https://doi.org/10.1016/0040-1951\(95\)00003-6](https://doi.org/10.1016/0040-1951(95)00003-6), 1995.
- 625 Burbank, D. W. and Anderson, R. S.: Tectonic geomorphology, 2nd ed., J. Wiley & Sons, Chichester, West Sussex, Hoboken, N.J., 454 pp., 2012.
- Büttner, S. H.: Late Variscan stress-field rotation initiating escape tectonics in the south-western Bohemian Massif: a far field response to late-orogenic extension, J. Geosci., 52, 29–43, <https://doi.org/10.3190/jgeosci.004>, 2007.
- Carlé, W.: Bau und Entwicklung der Südwestdeutschen Großscholle, Beihefte zum Geologischen Jahrbuch, 16, Schweizerbart  
630 Science Publishers, Stuttgart, 272 pp., 1955.
- Chen, F. and Siebel, W.: Zircon and titanite geochronology of the Furstenstein granite massif, Bavarian Forest, NW Bohemian Massif: Pulses of the late Variscan magmatic activity, Eur. J. Mineral., 16, 777–788, <https://doi.org/10.1127/0935-1221/2004/0016-0777>, 2004.
- Chen, F., Siebel, W., and Satir, M.: Geochemical and isotopic composition and inherited zircon ages as evidence for lower  
635 crustal origin of two Variscan S-type granites in the NW Bohemian massif, Int. J. Earth Sci. (Geol. Rundsch.), 92, 173–184, <https://doi.org/10.1007/s00531-003-0310-6>, 2003.
- Chen, G.-N. and Grapes, R.: Granite Genesis: In-Situ Melting and Crustal Evolution, Springer Science+Business Media B.V., Dordrecht, 2007.



- 640 Cymerman, Z., Piasecki, M. A. J., and Seston, R.: Terranes and terrane boundaries in the Sudetes, northeast Bohemian Massif, *Geol. Mag.*, 134, 717–725, <https://doi.org/10.1017/S0016756897007255>, 1997.
- Daurer, A.: Das Moldanubikum im Bereich der Donaustörung zwischen Jochenstein und Schlögen (Oberösterreich), *Mitt. Ges. Geol. Bergbaustud. Österr.*, 23, 1–54, 1976.
- Davis, J. C.: *Statistics and data analysis in geology*, 3rd ed., Wiley, New York, 638 pp., 2002.
- de Wall, H., Schaarschmidt, A., Kämmlin, M., Gabriel, G., Bestmann, M., and Scharfenberg, L.: Subsurface granites in the Franconian Basin as the source of enhanced geothermal gradients: a key study from gravity and thermal modeling of the Bayreuth Granite, *Int. J. Earth Sci. (Geol. Rundsch.)*, 108, 1913–1936, <https://doi.org/10.1007/s00531-019-01740-8>, 2019.
- 645 Dietl, C., Gößmann, M., and de Wall, H.: Kombinierte aktive und passive Plutonplatznahme in einer verdickten Kruste - Erste Ergebnisse von gesteinsmagnetischen und petrologischen Untersuchungen am Fürstensteiner Intrusivkomplex (Bayerischer Wald), *Z. dt. geol. Ges.*, 155, 311–328, 2005.
- 650 Drury, S. A.: *Image interpretation in geology*, 2. ed., Chapman & Hall, London, 283 pp., 1987.
- Echtler, H. P. and Chauvet, A.: Carboniferous convergence and subsequent crustal extension in the southern Schwarzwald (SW Germany), *Geodin. Acta*, 5, 37–49, <https://doi.org/10.1080/09853111.1992.11105218>, 1992.
- Fatka, O. and Mergl, M.: The ‘microcontinent’ Perunica: status and story 15 years after conception, *Geol. Soc. Spec. Publ.*, 325, 65–101, <https://doi.org/10.1144/SP325.4>, 2009.
- 655 Finger, F. and Rene, M.: A Comment on 'Two Distinctive Granite Suites in the SW Bohemian Massif and their Record of Emplacement: Constraints from Geochemistry and Zircon 207Pb/206Pb Chronology' by Siebel et al. *Journal of Petrology* 49, 1853–1872, *J. Petrol.*, 50, 591–593, <https://doi.org/10.1093/petrology/egp013>, 2009.
- Finger, F. and Clemens, J. D.: Migmatization and "secondary" granitic magmas: effects of emplacement and crystallization of "primary" granitoids in Southern Bohemia, Austria, *Contrib. Mineral. and Petrol.*, 120, 311–326, <https://doi.org/10.1007/BF00306510>, 1995.
- 660 Finger, F., Dunkley, D. J., and René, M.: Remnants of Early Carboniferous I-type granodiorite plutons in the Bavarian Forest and their bearing on the tectonic interpretation of the south-western sector of the Bohemian Massif (Bavarian Zone), *J. Geosci.*, 55, 321–332, <https://doi.org/10.3190/jgeosci.080>, 2010.
- Finger, F., Gerdes, A., Janoušek, V., René, M., and Riegler, G.: Resolving the Variscan evolution of the Moldanubian sector of the Bohemian Massif: the significance of the Bavarian and the Moravo-Moldanubian tectonometamorphic phases, *J. Geosci.*, 52, 9–28, <https://doi.org/10.3190/jgeosci.005>, 2007.
- 665 Franke, W.: The mid-European segment of the Variscides: tectonostratigraphic units, terrane boundaries and plate tectonic evolution, *Geol. Soc. Spec. Publ.*, 179, 35–61, <https://doi.org/10.1144/GSL.SP.2000.179.01.05>, 2000.
- Franke, W.: Tectonostratigraphic units in the Variscan belt of central Europe, in: *Terranes in the Circum-Atlantic Paleozoic Orogens*, edited by: Dallmeyer, R. D., Geological Society of America, Boulder, Colo., 67–90, <https://doi.org/10.1130/SPE230-p67>, 1989.
- 670



- Freudenberger, W.: Tektonik, in: Erläuterungen zur Geologischen Karte von Bayern 1:500 000, 4th ed., edited by: Bayerisches Geologisches Landesamt, München, 259–265, 1996.
- Freudenberger, W. and Schwerd, K.: Tektonische Karte von Bayern 1:1000000, in: Erläuterungen zur Geologischen Karte von Bayern 1:500 000, 4th ed., edited by: Bayerisches Geologisches Landesamt, München, 1996.
- 675 Führer, F. X.: Die Anomalien der Schwere am Südwest-Rand des Bayerischen Waldes und ihre Interpretation, *Int. J. Earth Sci. (Geol. Rundsch.)*, 67, 1078–1096, <https://doi.org/10.1007/BF01983255>, 1978.
- Fürst, M., Krupp, R., and Müller, R.: Die photogeologische Linearanalyse und ihre Anwendung bei der Uranprospektion in der Oberpfalz, *Erlanger geol. Abh.*, 3–33, 1978.
- 680 Galadí-Enríquez, E., Dörr, W., Zulauf, G., Galindo-Zaldívar, J., Heidelberg, F., and Rohrmüller, J.: Variscan deformation phases in the southwestern Bohemian Massif: new constraints from sheared granitoids, *Z. dt. Ges. Geowiss.*, 161, 1–23, <https://doi.org/10.1127/1860-1804/2010/0161-0001>, 2010.
- Galadí-Enríquez, E., Kroemer, E., Loth, G., Pürner, T., Raum, G., Teipel, U., and Rohrmüller, J.: Erdgeschichte des Oberpfälzer Waldes: Geologischer Bau, Gesteine, Sehenswürdigkeiten, Erläuterungen zur Geologischen Karte des Oberpfälzer Waldes, Augsburg, 2009a.
- 685 Galadí-Enríquez, E., Kroemer, E., Loth, G., Pürner, T., Raum, G., Teipel, U., and Rohrmüller, J.: Geologische Karte des Oberpfälzer Waldes 1:150000, Bayerisches Landesamt für Umwelt, Augsburg, 2009b.
- Gebauer, D.: Erdgeschichtliche Entwicklung und geologischer Überblick, in: *Erl. Geol. Kt. Bayern 1:25.000*, Bl. 7446 Passau, edited by: Bauberger, W. and Unger, H. J., München, 13–22, 1984.
- 690 Gerdes, A., Finger, F., and Parrish, R. R.: Southwestward progression of a late-orogenic heat front in the Moldanubian Zone of the Bohemian Massif and formation of the Austro-Bavarian anatexite belt, *Geophys. Res. Abstr.*, 8, 2006.
- Goldsworthy, M. and Jackson, J.: Active normal fault evolution in Greece revealed by geomorphology and drainage patterns, *J. Geol. Soc.*, 157, 967–981, <https://doi.org/10.1144/jgs.157.5.967>, 2000.
- Grauert, B., Hányi, R., and Soptrajanova, G.: Geochronology of a Polymetamorphic and Anatectic Gneiss Region: The Moldanubicum of the Area Lam-Deggendorf, Eastern Bavaria, Germany, *Contrib. Mineral. and Petrol.*, 45, 37–63, <https://doi.org/10.1007/BF00371136>, 1974.
- 695 Guy, A., Edel, J.-B., Schulmann, K., Tomek, Č., and Lexa, O.: A geophysical model of the Variscan orogenic root (Bohemian Massif): Implications for modern collisional orogens, *Lithos*, 124, 144–157, <https://doi.org/10.1016/j.lithos.2010.08.008>, 2011.
- 700 Healy, D., Rizzo, R. E., Cornwell, D. G., Farrell, N. J., Watkins, H., Timms, N. E., Gomez-Rivas, E., and Smith, M.: FracPaQ: A MATLAB™ toolbox for the quantification of fracture patterns, *J. Struct. Geol.*, 95, 1–16, <https://doi.org/10.1016/j.jsg.2016.12.003>, 2017.



- 705 Hejl, E., Coyle, D., Lal, N., van den haute, P., and Wagner, G. A.: Fission-track dating of the western border of the Bohemian massif: thermochronology and tectonic implications, *Int. J. Earth Sci. (Geol. Rundsch.)*, 86, 210–219, <https://doi.org/10.1007/s005310050133>, 1997.
- Horn, P., Köhler, H., and Müller-Sohnius, D.: Rb-Sr-isotopengeochemie hydrothermaler quarze des bayerischen pfahles und eines flusspat-schwerspatganges von nabburg-wölsendorf/bundesrepublik deutschland, *Chemical Geology: Isotope Geoscience section*, 58, 259–272, [https://doi.org/10.1016/0168-9622\(86\)90015-1](https://doi.org/10.1016/0168-9622(86)90015-1), 1986.
- 710 Jordan, G., Meijninger, B., van Hinsbergen, D., Meulenkamp, J. E., and Van Dijk, P. M.: Extraction of morphotectonic features from DEMs: Development and applications for study areas in Hungary and NW Greece, *Int. J. Appl. Earth Obs. Geoinf.*, 7, 163–182, <https://doi.org/10.1016/j.jag.2005.03.003>, 2005.
- Kalt, A., Berger, A., and Blümel, P.: Metamorphic Evolution of Cordierite-Bearing Migmatites from the Bayerische Wald (Variscan Belt, Germany), *J. Petrol.*, 40, 601–627, <https://doi.org/10.1093/petroj/40.4.601>, 1999.
- 715 Kalt, A., Corfu, F., and Wijbrans, J. R.: Time calibration of a P-T path from a Variscan high-temperature low-pressure metamorphic complex (Bayerische Wald, Germany), and the detection of inherited monazite, *Contrib. Mineral. and Petrol.*, 138, 143–163, <https://doi.org/10.1007/s004100050014>, 2000.
- Keller, E. A. and Pinter, N.: *Active tectonics: Earthquakes, uplift, and landscape*, 2nd ed., Prentice Hall earth science series, Prentice Hall, Upper Saddle River NJ, XIII, 362 S, 2002.
- 720 Klein, T., Kiehm, S., Siebel, W., Shang, C. K., Rohrmüller, J., Dörr, W., and Zulauf, G.: Age and emplacement of late-Variscan granites of the western Bohemian Massif with main focus on the Hauzenberg granitoids (European Variscides, Germany), *Lithos*, 102, 478–507, <https://doi.org/10.1016/j.lithos.2007.07.025>, 2008.
- Kley, J. and Voigt, T.: Late Cretaceous intraplate thrusting in central Europe: Effect of Africa-Iberia-Europe convergence, not Alpine collision, *Geology*, 36, 839–842, <https://doi.org/10.1130/G24930A.1>, 2008.
- 725 Klominský, J., Jarchovský, T., and Rajpoot, G. S.: *ATLAS of plutonic rocks and orthogneisses in the Bohemian Massif: MOL DANUBICUM*, Czech Geological Survey, Prague, 2010.
- Kossmat, F.: *Gliederung des varistischen Gebirgebaus*, *Abhandlungen des Sächsischen Geologischen Landesamts*, 1, 1–39, 1927.
- Krohe, A.: Variscan tectonics of central Europe: Postaccretionary intraplate deformation of weak continental lithosphere, *Tectonics*, 15, 1364–1388, <https://doi.org/10.1029/96TC01110>, 1996.
- 730 Kroner, U. and Romer, R. L.: Two plates — Many subduction zones: The Variscan orogeny reconsidered, *Gondwana Research*, 24, 298–329, <https://doi.org/10.1016/j.gr.2013.03.001>, 2013.
- Kroner, U., Mansy, J.-L., Mazur, S., Aleksandrowski, P., Hann, H. P., Huckriede, H., Lacquement, F., Lamarche, J., Ledru, P., Pharaoh, T. C., Zedler, H., Zeh, A., and Zulauf, G.: Variscan Tectonics, in: *The geology of Central Europe: Volume 1: Precambrian and Palaeozoic*, edited by: McCann, T., The Geological Society London, London, 599–664, 2008.



- 735 Leibniz-Institut für Angewandte Geophysik: Schwerekarte der Bundesrepublik Deutschland 1:1 000 000, Bouguer Anomalien,  
Liag, Hannover, 2010.
- Linnemann, U., McNaughton, N. J., Romer, R. L., Gehmlich, M., Drost, K., and Tonk, C.: West African provenance for Saxo-  
Thuringia (Bohemian Massif): Did Armorica ever leave pre-Pangean Gondwana? ? U/Pb-SHRIMP zircon evidence and  
the Nd-isotopic record, *Int. J. Earth Sci. (Geol. Rundsch.)*, 93, 683–705, <https://doi.org/10.1007/s00531-004-0413-8>, 2004.
- 740 Lowrie, W.: *Fundamentals of Geophysics*, 2. ed., 4th printing, Cambridge Univ. Press, Cambridge, 381 pp., 2007.
- Matte, P.: Tectonics and plate tectonics model for the Variscan belt of Europe, *Tectonophysics*, 126, 329–374,  
[https://doi.org/10.1016/0040-1951\(86\)90237-4](https://doi.org/10.1016/0040-1951(86)90237-4), 1986.
- Mattern, F.: Late Carboniferous to early Triassic shear sense reversals at strike-slip faults in eastern Bavaria, *Zbl Geol Paläon-  
tol Teil I*, 1993, 1471–1490, 1995.
- 745 Meyer, R. K. F.: Tektonik des Deckgebirges, in: *Erl. Geol. Kt. Bayern 1:25.000*, Bl. 6639 Wackersdorf, edited by: Meyer, R.  
K. F. and Mielke, H., 118–121, 1993.
- Meyer, R. K. F.: Die Entwicklung der Pfahl-Störungszone und des Bodenwöhler Halbgrabens auf Blatt Wackersdorf, *Erlanger  
geol. Abh.*, 117, 1–24, 1989.
- Mielke, H.: Geologische Entwicklung des Kristallins, in: *Erl. Geol. Kt. Bayern 1:25.000*, Bl. 6639 Wackersdorf, edited by:  
750 Meyer, R. K. F. and Mielke, H., 10–12, 1993.
- Müller, M.: Neue Vorstellungen zur Entwicklung des Nordostbayerischen Permokarbon-Trogs aufgrund reflexionsseismischer  
Messungen in der Mittleren Oberpfalz, *Geol. Bl. NO-Bayern*, 44, 195–224, 1994.
- Neubauer, F. and Handler, R.: Variscan orogeny in the Eastern Alps and Bohemian Massif: How do these units correlate?,  
*Mitt. Österr. Geol. Ges.*, 92, 35–59, 2000.
- 755 Pérez-Peña, J. V., Al-Awabdeh, M., Azañón, J. M., Galve, J. P., Booth-Rea, G., and Notti, D.: SwathProfiler and NProfiler:  
Two new ArcGIS Add-ins for the automatic extraction of swath and normalized river profiles, *Comput. Geosci.*, 104, 135–  
150, <https://doi.org/10.1016/j.cageo.2016.08.008>, 2017.
- Peterek, A., Rauche, H., Schröder, B., Franzke, H.-J., Bankwitz, P., and Bankwitz, E.: The late-and post-Variscan tectonic  
evolution of the Western Border fault zone of the Bohemian massif (WBZ), *Int. J. Earth Sci. (Geol. Rundsch.)*, 86, 191–  
760 202, <https://doi.org/10.1007/s005310050131>, 1997.
- Peterek, A., Schröder, B., and Menzel, D.: Zur postvariszischen Krustenentwicklung des Naabgebirges und seines Rahmens,  
*Z. geol. Wiss.*, 24, 293–304, 1996.
- Petkovic, P.: Gravity and granites technical notes on mapping relationships of known granites and gravity, *Record 2014/012*,  
*Geoscience Australia*, <https://doi.org/10.11636/Record.2014.012>, 2014.
- 765 Priehäusser, G.: Felsfreistellungen, Blockmeere, Blockströme und Blockstreuungen im Bayer. Wald, *Geol. Bl. NO-Bayern*,  
11, 123–132, 1961.





- Propach, G., Baumann, A., Schulz-Schmalschläger, M., and Grauert, B.: Zircon and monazite U-Pb ages of Variscan granitoid rocks and gneisses in the Moldanubian zone of eastern Bavaria, Germany, *N. Jb. Geol. Paläont. Mh.*, 2000, 345–377, <https://doi.org/10.1127/njgpm/2000/2000/345>, 2000.
- 770 Prost, G. L.: *Remote Sensing for Geologists: A Guide to Image Interpretation*, Gordon and Breach Science Publishers, Amsterdam, 326 pp., 1994.
- Rohrmüller, J., Artmann, C., and Teipel, U.: Das kristalline Grundgebirge des Moldanubikums von der Donau bis zur Pfahlzone (Exkursion L am 21. April 2017): The crystalline basement of the Moldanubian from the Danube to the Bavarian Pfahl Zone, *Jber. Mitt. oberrhein. geol. Ver.*, 99, 345–370, <https://doi.org/10.1127/jmoggv/99/0011>, 2017.
- 775 Rohrmüller, J., Mielke, H., and Gebauer, D.: Gesteinsfolge des Grundgebirges nördlich der Donau und im Molasseuntergrund, in: *Erläuterungen zur Geologischen Karte von Bayern 1:500 000*, 4th ed., edited by: Bayerisches Geologisches Landesamt, München, 16–54, 1996.
- Rosenberg, C. L.: Shear zones and magma ascent: A model based on a review of the Tertiary magmatism in the Alps, *Tectonics*, 23, <https://doi.org/10.1029/2003TC001526>, 2004.
- 780 Schaarschmidt, A., Haase, K. M., de Wall, H., Bestmann, M., Krumm, S., and Regelous, M.: Upper crustal fluids in a large fault system: microstructural, trace element and oxygen isotope study on multi-phase vein quartz at the Bavarian Pfahl, SE Germany, *Int. J. Earth Sci. (Geol. Rundsch.)*, 108, 521–543, <https://doi.org/10.1007/s00531-018-1666-y>, 2019.
- Scheiber, T., Fredin, O., Viola, G., Jarna, A., Gasser, D., and Łapińska-Viola, R.: Manual extraction of bedrock lineaments from high-resolution LiDAR data: methodological bias and human perception, *GFF*, 137, 362–372, <https://doi.org/10.1080/11035897.2015.1085434>, 2015.
- 785 Schröder, B.: Outline of the Permo-Carboniferous basins at the western margin of the Bohemian Massif, *Z. geol. Wiss.*, 16, 993–1001, 1988.
- Schulmann, K., Catalán, J. R. M., Lardeaux, J. M., Janoušek, V., and Oggiano, G.: The Variscan orogeny: extent, timescale and the formation of the European crust, *Geol. Soc. Spec. Publ.*, 405, 1–6, <https://doi.org/10.1144/SP405.15>, 2014.
- 790 Sedlák, J., Gnojek, I., Scheibe, R., and Zabadal, S.: Gravity response of igneous rocks in the northwestern part of the Bohemian Massif, *J. Geosci.*, 54, 325–342, <https://doi.org/10.3190/jgeosci.054>, 2009.
- Sedlák, J., Gnojek, I., Zabadal, S., Farbisz, J., Cwojdzinski, S., and Scheibe, R.: Geological interpretation of a gravity low in the central part of the Lugian Unit (Czech Republic, Germany and Poland), *J. Geosci.*, 52, 181–197, <https://doi.org/10.3190/jgeosci.012>, 2007.
- 795 Seemann, R.: Die geologischen Verhältnisse längs der Amberg-Sulzbacher und Auerbacher-Pegnitzer Störung, *Abh. naturhist. Ges. Nürnberg*, 22, 93–149, 1925.
- Siebel, W., Shang, C. K., Thern, E., Danišik, M., and Rohrmüller, J.: Zircon response to high-grade metamorphism as revealed by U–Pb and cathodoluminescence studies, *Int. J. Earth Sci. (Geol. Rundsch.)*, 101, 2105–2123, <https://doi.org/10.1007/s00531-012-0772-5>, 2012.



- 800 Siebel, W., Hann, H. P., Danišik, M., Shang, C. K., Berthold, C., Rohrmüller, J., Wemmer, K., and Evans, N. J.: Age constraints on faulting and fault reactivation: a multi-chronological approach, *Int. J. Earth Sci. (Geol. Rundsch.)*, 99, 1187–1197, <https://doi.org/10.1007/s00531-009-0474-9>, 2010.
- Siebel, W., Shang, C. K., Reitter, E., Rohrmüller, J., and Breiter, K.: Two Distinctive Granite Suites in the Southwestern Bohemian Massif: Reply to F. Finger and M. Rene, *J. Petrol.*, 50, 595–599, <https://doi.org/10.1093/petrology/egp012>, 2009.
- 805 Siebel, W., Shang, C. K., Reitter, E., Rohrmüller, J., and Breiter, K.: Two Distinctive Granite Suites in the SW Bohemian Massif and their Record of Emplacement: Constraints from Geochemistry and Zircon 207Pb/206Pb Chronology, *J. Petrol.*, 49, 1853–1872, <https://doi.org/10.1093/petrology/egn049>, 2008.
- Siebel, W., Thiel, M., and Chen, F.: Zircon geochronology and compositional record of late- to post-kinematic granitoids associated with the Bavarian Pfahl zone (Bavarian Forest), *Mineral. Petrol.*, 86, 45–62, <https://doi.org/10.1007/s00710-005-0091-7>, 2006a.
- 810 Siebel, W., Hann, H. P., Shang, C. K., Rohrmüller, J., and Chen, F.: Coeval late-Variscan emplacement of granitic rocks: an example from the Regensburg Forest, NE Bavaria, *N. Jb. Miner. Abh.*, 183, 13–26, <https://doi.org/10.1127/0077-7757/2006/0058>, 2006b.
- 815 Siebel, W., Blaha, U., Chen, F., and Rohrmüller, J.: Geochronology and geochemistry of a dyke-host rock association and implications for the formation of the Bavarian Pfahl shear zone, Bohemian Massif, *Int. J. Earth Sci. (Geol. Rundsch.)*, 94, 8–23, <https://doi.org/10.1007/s00531-004-0445-0>, 2005.
- Siebel, W., Chen, F., and Satir, M.: Late-Variscan magmatism revisited: new implications from Pb-evaporation zircon ages on the emplacement of redwitzites and granites in NE Bavaria, *Int. J. Earth Sci. (Geol. Rundsch.)*, 92, 36–53, <https://doi.org/10.1007/s00531-002-0305-8>, 2003.
- 820 Siebel, W., Trzebski, R., Stettner, G., Hecht, L., Casten, U., Höhndorf, A., and Müller, P.: Granitoid magmatism of the NW Bohemian massif revealed: gravity data, composition, age relations and phase concept, *Int. J. Earth Sci. (Geol. Rundsch.)*, 86, 45–63, <https://doi.org/10.1007/PL00014665>, 1997.
- 825 Skiba, P.: Homogene Schwerekarte der Bundesrepublik Deutschland (Bouguer-Anomalien). Technischer Bericht zur Fortführung der Datenbasis, deren Auswertung und Visualisierung, LIAG-Bericht, Hannover, 2011.
- Smithson, S. B.: Densities of metamorphic rocks, *Geophysics*, 36, 690–694, <https://doi.org/10.1190/1.1440205>, 1971.
- Stephan, T., Kroner, U., Hahn, T., Hallas, P., and Heuse, T.: Fold/cleavage relationships as indicator for late Variscan sinistral transpression at the Rheno-Hercynian–Saxo-Thuringian boundary zone, Central European Variscides, *Tectonophysics*, 681, 250–262, <https://doi.org/10.1016/j.tecto.2016.03.005>, 2016.
- 830 Stewart, S. I. and Hancock, P. L.: What is a fault scarp?, *Episodes*, 4, 256–263, 1990.
- Teipel, U., Galadí-Enríquez, E., Glaser, S., Kroemer, E., and Rohrmüller, J.: Geologische Karte des Bayerischen Waldes 1:150000, Bayerisches Landesamt für Umwelt, Augsburg, 2008.



- Telbisz, T., Kovács, G., Székely, B., and Szabó, J.: Topographic swath profile analysis: a generalization and sensitivity evaluation of a digital terrain analysis tool, *Z. Geomorphol.*, 57, 485–513, <https://doi.org/10.1127/0372-8854/2013/0110>, 2013.
- 835 Toloczyki, M., Trurnit, P., Voges, A., Wittekindt, H., and Zitzmann, A.: Geologische Karte der Bundesrepublik Deutschland 1:1.000.000 (GK1000), Bundesanstalt für Geowissenschaften und Rohstoffe, Hannover, 2006.
- Troll, G.: Die blastokataklastischen Kristallingesteine der Stallwanger Furche, Bayerischer Wald, in: *Geologica Bavarica* Nr. 58: Führer zu geologisch-petrographischen Exkursionen im Bayerischen Wald, edited by: Bayerisches Geologisches Landesamt, München, 22–33, 1967.
- 840 Trzebski, R., Behr, H. J., and Conrad, W.: Subsurface distribution and tectonic setting of the late-Variscan granites in the northwestern Bohemian Massif, *Int. J. Earth Sci. (Geol. Rundsch.)*, 86, 64-78, <https://doi.org/10.1007/PL00014666>, 1997.
- Vamvaka, A., Siebel, W., Chen, F., and Rohrmüller, J.: Apatite fission-track dating and low-temperature history of the Bavarian Forest (southern Bohemian Massif), *Int. J. Earth Sci. (Geol. Rundsch.)*, 103, 103–119, <https://doi.org/10.1007/s00531-013-0945-x>, 2014.
- 845 Vercoutere, C.: The Thermotectonic History of the Brabant Massif (Belgium) and the Naab Basement (Germany) : an Apatite Fission Track Analysis, PhD thesis, Faculteit Wetenschappen, Universiteit Gent, Gent, 1994.
- Wagner, G. A., Coyle, D. A., Duyster, J., Henjes-Kunst, F., Peterek, A., Schröder, B., Stöckhert, B., Wemmer, K., Zulauf, G., Ahrendt, H., Bischoff, R., Hejl, E., Jacobs, J., Menzel, D., Lal, N., van den haute, P., Vercoutere, C., and Welzel, B.: Post-Variscan thermal and tectonic evolution of the KTB site and its surroundings, *J. Geophys. Res.*, 102, 18221–18232, <https://doi.org/10.1029/96JB02565>, 1997.
- 850 Wagner, G. A., Michalski, I., and Zaun, P.: Apatite Fission Track Dating of the Central European Basement. Postvariscan Thermo-Tectonic Evolution, in: *The German continental deep drilling program (KTB): Site selection studies in the Oberpfalz and Schwarzwald*, edited by: Emmermann, R., Springer, Berlin, Heidelberg, New York, London, Paris, Tokyo, Hong Kong, 481–500, 1989.
- 855 Wallbrecher, V. E., Dallmeyer, R. D., Brandmayr, M., Handler, R., Maderbacher, F., and Platzer, R.: Kinematik und Alter der Blattverschiebungszonen in der südlichen Böhmisches Masse, in: *Arbeitstagung Geol. B.-A.*, edited by: Gattiner, T. E. and Roetzel, R., Verlag d. Geologischen Bundesanstalt, 1991.
- Weinberg, R. F., Sial, A. N., and Mariano, G.: Close spatial relationship between plutons and shear zones, *Geol. Soc. Am. Bull.*, 32, 377–380, <https://doi.org/10.1130/G20290.1>, 2004.
- 860 Wimmenauer, W. and Bryhni, I.: A systematic nomenclature for metamorphic rocks: Migmatites and related rocks, A proposal on behalf of the IUGS Subcommittee on the Systematics of Metamorphic Rocks, Web version of 01.02.2007, 2007.
- Žák, J. and Sláma, J.: How far did the Cadomian ‘terranes’ travel from Gondwana during early Palaeozoic? A critical reappraisal based on detrital zircon geochronology, *International Geology Review*, 60, 319–338, <https://doi.org/10.1080/00206814.2017.1334599>, 2018.



- 865 Žák, J., Verner, K., Janoušek, V., Holub, F. V., Kachlík, V., Finger, F., Hajná, J., Tomek, F., Vondrovic, L., and Trubač, J.: A  
plate-kinematic model for the assembly of the Bohemian Massif constrained by structural relationships around granitoid  
plutons, *Geol. Soc. Spec. Publ.*, 405, 169–196, <https://doi.org/10.1144/SP405.9>, 2014.
- Zeitlhöfler, M.: Brittle Petrofabrics in the Central Bavarian Forest (SE Germany): Tectonic Evolution, Geomorphological  
Effects, and Hydrogeologic Implications, PhD thesis, Fakultät für Geowissenschaften, Ludwig-Maximilians-Universität  
870 München, München, 445 pp., 2007.